Published in final edited form as:

Phys Med Biol. ; 64(4): 04TR01. doi:10.1088/1361-6560/aaf4de.

Radioluminescence in Biomedicine: Physics, Applications, and Models

Justin Klein[1], **Conroy Sun**[2], and **Guillem Pratx**[1,*]

[1]Department of Radiation Oncology, Stanford University, Stanford, CA 94305

[2]College of Pharmacy, Oregon State University, Portland, OR 97201

Abstract

The electromagnetic spectrum contains different frequency bands useful for medical imaging and therapy. Short wavelengths (ionizing radiation) are commonly used for radiological and radionuclide imaging and for cancer radiation therapy. Intermediate wavelengths (optical radiation) are useful for more localized imaging and for photodynamic therapy. Finally, longer wavelengths are the basis for magnetic resonance imaging and for hyperthermia treatments. Recently, there has been a surge of interest for new biomedical methods that synergize optical and ionizing radiation by exploiting the ability of ionizing radiation to stimulate optical emissions. These physical phenomena, together known as radioluminescence, are being used for applications as diverse as radionuclide imaging, radiation therapy monitoring, phototherapy, and nanoparticle-based molecular imaging. This review provides a comprehensive treatment of the physics of radioluminescence and includes simple analytical models to estimate the luminescence yield of scintillators and nanoscintillators, Cerenkov radiation, air fluorescence, and biologically endogenous radioluminescence. Examples of methods that use radioluminescence for diagnostic or therapeutic applications are reviewed and analyzed in light of these quantitative physical models of radioluminescence.

Keywords

Radioluminescence; biomedical imaging; radiation therapy; Cerenkov luminescence; scintillators; nanotechnology

1 Introduction

Radioluminescence is the production of optical photons from the interaction of ionizing radiation with matter. It is a broad term that encompasses many phenomena caused by different physics. These include scintillation, Cerenkov radiation, and the induction of fluorescence, phosphorescence, and delayed/persistent luminescence by ionizing radiation.

While radiation detectors have leveraged scintillator-produced radioluminescence for decades, most sources of radioluminescence are so weak that their potential utility in

*Corresponding Author Guillem Pratx, PhD, Assistant Professor of Radiation Oncology, Stanford University School of Medicine, 300 Pasteur Dr, Grant S277, Stanford, CA 94305-5132, pratx@stanford.edu, 650-724-9829.

biomedicine has not been considered until recently. The prevalence of high sensitivity optical cameras now permits routine imaging of faint radioluminescent signals, even within living organisms.

Biomedical applications of radioluminescence broadly fall into two areas, depending on the intensity and duration of the radiation exposure: imaging or therapy. Imaging applications are feasible at low optical fluence rates while therapeutic ones necessitate high fluence rates over greater time durations to achieve a biological effect. The purpose of this review is to summarize the physics and applications of biomedically relevant sources of radioluminescence, to put fourth simple quantitative models for consideration of each phenomenon in the biomedical setting, and to speculate on their suitability for imaging and therapy applications.

The models described in this review are intended to serve as a quantitative framework for evaluating potential applications of radioluminescence. Due to their simplicity, they should be considered useful for order-of-magnitude estimation. Example calculations have been provided and different results may be obtained by changing the numerical values that have been assumed.

2 Cerenkov luminescence

2.1 Physics

Cerenkov radiation is an optical signal induced in dielectric media by fast, charged particles. It is a threshold effect occurring when a charged particle exceeds the phase velocity of light in that medium. The threshold is approximately 214 keV in water and 261 keV in tissue. Cerenkov radiation is induced by successive polarization and depolarization of the medium along the charged particle trajectory, which gives rise to constructive interferences (Jelley 1958).

The Cerenkov photon yield is computed using the Frank-Tamm formula (Mitchell et al 2011):

$$\frac{dN}{dx} = 2\pi\alpha\left(1 - \frac{1}{n^2\beta^2}\right)\int_{\lambda_1}^{\lambda_2} \frac{1}{\lambda^2}\, d\lambda \quad (1)$$

where $\frac{dN}{dx}$ is the number of photons emitted per fractional step length of a charged particle in a dielectric medium; n is the refractive index of the medium; β is the ratio of the velocity of the charged particle to the vacuum speed of light; and $\alpha = 1/137$ is the fine structure constant. The emitted photons are, in practice, limited to wavelengths above 100 nm by refractive indices that decrease with wavelength in real dielectric materials (Jelley 1958).

Cerenkov radiation possesses unique spectral, spatial, and polarization properties. Its emission spectrum is continuous from the infrared to ultraviolet region and proportional to $1/\lambda^2$ (Figure 1). Cerenkov photons are emitted anisotropically from the charged particle,

following a cone-shaped distribution aligned with the direction of the travelling particle. The angle (θ) of the Cerenkov cone is directly related to the velocity of the charged particle, according to: $\cos\theta = \frac{1}{n\beta}$.

The physics and history of Cerenkov radiation have been exhaustively covered in (Jelley 1958), and biomedical applications are summarized in recent reviews (Grimm 2015, Tanha *et al* 2015, Ciarrocchi and Belcari 2017). The following section considers several pre-clinical and clinical applications, along with their current limitations.

2.2 Applications

2.2.1 Time-of-flight PET detectors—CL has been explored as a timing signal for time-of-flight (TOF) PET detectors. CL is generated promptly in the scintillator from recoil electrons and has lower transit time uncertainty compared to scintillation photons (Lecoq *et al* 2010). Proof-of-concept experiments have shown 71 ps timing resolution based on coincidence detection of the Cerenkov signal (Korpar *et al* 2011). BGO-based PET detectors have been developed (Kwon *et al* 2016, Brunner and Schaart 2017). They generate both Cerenkov and scintillation photons; the earliest arriving Cerenkov photons provide coincidence timing while later scintillation photons are used for energy discrimination. This hybrid detector harnesses the benefits of BGO (high stopping power, photoelectric fraction, no background radiation, lower cost), while overcoming timing resolution limitations.

2.2.2 Cerenkov luminescence imaging—*Cerenkov luminescence imaging* (CLI) is defined as optical imaging of Cerenkov radiation from radionuclides and radiotherapy beams. CLI is a direct method of imaging radionuclides otherwise only detectable with positron emission tomography (PET). All existing PET radionuclides and most beta-emitting radionuclides are sufficiently energetic to induce Cerenkov radiation in biological tissue.

CLI has been most prevalent in the pre-clinical domain, owing to the limited penetration depth of light in tissue, with planar imaging being the most common application (Robertson *et al* 2009, Liu *et al* 2010a, Ruggiero *et al* 2010, Mitchell *et al* 2011). Pre-clinical tomographic (Li *et al* 2010) and endoscopic (Liu *et al* 2012, Carpenter *et al* 2014) CLI have been reported. The benefit of CLI for pre-clinical imaging is the low cost and simplicity of the instrumentation, compared to PET.

CLI has also shown promise for important clinical applications, such as radiotherapy quality assurance, radiotherapy dosimetry, and surgical guidance.

Quality assurance and dosimetry are routinely performed to verify the quality of a radiotherapy treatment plan before it is delivered to the patient. Given the correlation between radiation dose and the intensity of the resulting CL, it is possible to use CLI to obtain a two-dimensional dose profile of a radiation beam (Glaser *et al* 2014). Multiple two-dimensional views can be combined to obtain three-dimensional beam profiles and dosimetry for electrons (Helo *et al* 2014) and photons (Glaser *et al* 2013a, 2013b). In addition, CLI can detect, in real-time, gross treatment errors during radiation treatment

arising from hardware faults or patient mispositioning; it can also coarsely estimate skin surface dose (Jarvis *et al* 2014).

CLI of injected radiopharmaceuticals (e.g. ^{18}F-fluorodeoxyglucose, FDG) is also being explored to guide surgeries such as sentinel lymph node biopsy, tumor margin assessment, and tumor detection; its potential utility is supported by both theoretical (Klein *et al* 2017) and experimental evidence (Thorek *et al* 2014b, Hu *et al* 2015, Grootendorst *et al* 2016b). Though briefly covered below, a comprehensive review has been written on the clinical applications of CLI (Grootendorst *et al* 2016a).

The first reported use of CLI in humans was for imaging a therapeutic dose of ^{131}I in human thyroid (Spinelli *et al* 2013); ^{18}F-FDG-positive lymph nodes have also been imaged in the axilla of breast cancer patients, using diagnostic levels of radiotracer (Thorek *et al* 2014b). Four patients were imaged and CLI signal correlated with positive lymph node status determined by PET.

Another pilot study of four patients showed promise for detecting human gastrointestinal (GI) tract tumors (Hu *et al* 2015). The study used a custom endoscope coupled to a sensitive EMCCD camera to image ^{18}F-FDG during colonoscopy. The system made it possible to differentiate GI tumors from normal tissue, even when inflamed (occurring in one patient). The dark environment achievable inside internal body cavities makes endoscopy an attractive application of CLI due to the faint intensity of the signal.

An ongoing trial of CLI for margin detection during breast conserving surgery has demonstrated the potential of CLI for detecting positive tumor margins. Tissue samples from 12 patients were imaged with a commercial CLI imaging system, and the CLI signal correlated with histopathology in all patients with assessable margins (10 of 12). Two patients with small tumors and late imaging times had un-assessable margins due to absence of Cerenkov signal (Grootendorst *et al* 2016b).

Cerenkov luminescence can excite fluorophores *in vivo*, a process called Cerenkov radiation energy transfer or secondary Cerenkov-induced fluorescence imaging. High Stokes-shift nanoparticles (Dothager *et al* 2010, Liu *et al* 2010b, Volotskova *et al* 2015) or molecular fluorophores that emit at longer wavelengths provide increased imaging sensitivity deeper within tissues or unique molecular contrast (Thorek *et al* 2013). Negative contrast can also be achieved using light-absorbing contrast agents (Thorek *et al* 2014a). The combination of Cerenkov luminescence and nanoparticles has been reviewed in detail (Shaffer *et al* 2017).

Finally, a recent development in Cerenkov imaging is Cerenkov-excited luminescence scanned imaging (CELSI). CELSI uses a megavoltage photon sheet-beam to selectively induce Cerenkov luminescence in the imaged subject, similar to light-sheet microscopy or x-ray radioluminescence tomography techniques (Zhang *et al* 2015). When combined with a fluorescent oxygen-sensing contrast agent, spatial resolution <300 μm and nanomolar sensitivity, have been demonstrated up to 5 mm deep in tissue (Pogue *et al* 2018).

2.2.3 Cerenkov luminescence for cancer phototherapy—Photodynamic therapy (PDT) is a clinically deployed treatment in which a light-activated drug, called a

photosensitizer, is administered and subsequently activated locally using an external light source. The photosensitizer preferentially accumulates in cancer tissue and, when excited with light, catalyzes the formation of reactive oxygen species (ROS) such as singlet oxygen ($^1O_2$) and hydroxyl radical ($^{\bullet}OH$) (Ochsner 1997). ROS exert a therapeutic effect through oxidative damage of cellular membranes, DNA and organelles, leading to cell death (Dougherty *et al* 1998, Wilson and Patterson 1986). PDT has better spatial specificity than systemic chemotherapy because its effect is only achieved in tissues under illumination. However, the possible applications of PDT are fundamentally limited by the limited penetration depth of light in tissue.

Cerenkov luminescence has garnered immense interest as a potential light source that could elegantly address the light penetration limitation of PDT. This combination could quickly enter the clinic by leveraging existing, approved photosensitizers, radiopharmaceuticals, and radiotherapy protocols.

Cerenkov luminescence-activated PDT has been reported using both radionuclides (Kotagiri *et al* 2015, Hartl *et al* 2016, Kamkaew *et al* 2016) and radiotherapy beams (Ouyang *et al* 2016, Yoon *et al* 2017). Notably, Kotagiri and colleagues reported a remarkable *in vivo* therapeutic effect using a TiO_2-based nanoparticle (Kotagiri *et al* 2015).

However, theoretical and quantitative studies have cast doubt on the possibility of CL-activated PDT (Glaser *et al* 2015) and suggest that alternative mechanisms such as radiosensitization and direct beta excitation (Pratx 2017, Pratt *et al* 2018) explain the therapeutic effects reported in prior work. Our own quantitative analysis agrees with these findings. In the following section, we provide simple models for estimating: photon yield from Cerenkov-emitting sources, ROS yield, radiation dose, and expected therapeutic efficacy due to Cerenkov-PDT alone; these models have been applied to prior work and estimated values are summarized in Table 2.

2.3 Models

2.3.1 Computed Cerenkov photon yield from radiation sources—

Both analytical and Monte Carlo methods have been used to predict absolute Cerenkov yields from alpha- (Ackerman and Graves 2012) and beta-emitting radionuclides (Mitchell *et al* 2011, Beattie *et al* 2012, Gill *et al* 2015). There is general good agreement among computed values and experimental measurements. Most radionuclides emit 1 to 100 Cerenkov photons/decay, depending on the radionuclide and wavelength range considered (Gill *et al* 2015).

Cerenkov photon yields for alpha-emitting radionuclides have been computed using GEANT4 Monte Carlo simulation (Ackerman and Graves 2012). Due to their mass, alpha-emitting radionuclides have insufficient energy to directly generate CL (1673 MeV threshold) in tissue. The decay products of some alpha-emitting radionuclides produce CL, but they are not useful for biomedical imaging because CL is not proportional to radioactivity until the sample reaches equilibrium. ^{212}Bi and ^{213}Bi are considered the most suitable alpha-emitting radionuclides for imaging because they partially undergo beta decay, producing CL.

In vivo fluence rates have been estimated for radionuclides and radiotherapy sources (Glaser *et al* 2015). Monte Carlo simulations (GMOS) were used first to derive Green's functions for Cerenkov light fluence over a range of biologically-relevant scattering and absorption coefficients. *In vivo* fluence rates were computed by convolving Green's functions with a biologically relevant radionuclide activity concentration or radiotherapy beam dose rate. Typical *in vivo* fluence rates for radionuclides are on the order of nW/cm^2/MBq/g, while those from radiotherapy sources are on the order of μW/cm^2/Gy/s (Glaser *et al* 2015).

2.3.2 Cerenkov photon yield from radionuclides—The Cerenkov photon yield of a given radionuclide (unit: photons per decay) is tabulated in several reference reports (Ackerman and Graves 2012, Gill *et al* 2015). From these values, it is possible to estimate the number of Cerenkov photon emitted given the starting radioactivity (A_0, in Bq), half-life ($t_{½}$, in seconds) and decay time (t), by integrating the radioactive decay formula from time = 0 to t. This yields the following decay factor, which represents the mean number of decays per Bq of radioactivity:

$$\text{Decay factor}\left[\text{decays}\cdot Bq^{-1}\right] = \frac{1}{A_0}\int_0^t A_0 \times e^{-\frac{ln2}{t_{1/2}}t}\,dt \qquad (1)$$

$$\approx 1.44 \times t_{1/2}\ \ [s] \times \left(1 - 2^{-\frac{t}{t_{1/2}}}\right)$$

$$\approx 1.44 \times t_{1/2}\ \ [s], \quad \text{when} \quad t \gg t_{1/2}$$

This quantity can be multiplied by the relevant Cerenkov yield to determine the total number of emitted Cerenkov photons from an initial radionuclide activity of 1 Bq:

$$\text{Decay-adjusted Cerenkov yield}\left[\frac{\text{photons}}{\text{Bq}}\right] = \text{Decay factor}\left[\frac{\text{decays}}{\text{Bq}}\right] \times \text{Cerenkov yield}\left[\frac{\text{photons}}{\text{decay}}\right] \qquad (2)$$

Photon yields for common medical radionuclides are computed using Equation 2 (Table 1). "Decay-adjusted Cerenkov yield" is the total number of photons emitted after decay of 1 Bq of initial activity over a duration t; "Decay factor" (computed from Equation 1) is computed as a function of t and $t_{½}$; "Cerenkov yield" is the mean number of Cerenkov photons emitted per decay, factoring in the branching ratio (often <1).

Cerenkov photon yields from (Gill *et al* 2015) are computed in the 400 – 800 nm wavelength range and can be scaled into any valid wavelength range (λ_{min} to λ_{max}), according to the following scaling factor:

$$F = 800 \quad [\text{nm}] \times \left(\frac{1}{\lambda_{\min} \quad [\text{nm}]} - \frac{1}{\lambda_{\max} [\text{nm}]} \right) \quad (3)$$

Radionuclides can impart significant radiation dose to tissue and cause biological effects. In this context, it is important to distinguish between *radiotracer dose* and *radiation dose*. Radiotracer dose corresponds to the amount of radioactivity administered to the subject and is given in units of Becquerel (Bq), which is defined the radioactivity of a substance that decays at a rate of one disintegration per second. In contrast, radiation dose is given in units of Gray (Gy) and is defined as the amount of ionizing energy (in Joules) deposited per kg of tissue. The relationship between radiotracer dose and radiation dose is complex and depends on many factors, such as the physical half-life of the radiotracer, its energy, its rate of uptake and excretion from different organs, and the type of radiation (alpha, beta, or gamma).

For the simple case of a beta-emitting radiotracer, radiation dose can be estimated by assuming that the entire kinetic energy of beta particles is deposited into the tissue volume of interest. This neglects the contribution of gamma rays that may be emitted from outside this volume. The radiation dose (in Gy, equivalent to J/kg) is:

$$\begin{aligned} \text{Dose [Gy]} = \quad & \text{Radioactivity concentration} \left[\frac{\text{Bq}}{\text{cm}^3} \right] \times \text{Decay factor} \left[\frac{\text{decays}}{\text{Bq}} \right] \\ & \times E_{\text{mean}} \left[\frac{\text{MeV}}{\text{decay}} \right] \times 1.6 \cdot 10^{-13} \quad \left[\frac{\text{J}}{\text{MeV}} \right] \times 10^3 \quad \left[\frac{\text{g}}{\text{kg}} \right] \times \frac{1}{\rho_{tissue}} \quad \left[\frac{\text{cm}^3}{\text{g}} \right] \end{aligned} \quad (4)$$

where *radioactivity concentration* is that contained in the considered tissue; E_{mean} is the mean kinetic energy of the emitted beta particles and ρ_{tissue} is tissue density (typically 1 g/cm^3). This formula is most accurate when the spatial dimensions of the volume of interest are large compared to particle range (typically ~mm); as volume becomes small, it will tend to overestimate dose due to the incorrect assumption that all energy is deposited within the volume.

2.3.3 Cerenkov photon yield from radiotherapy source—The Cerenkov photon yield (noted R_E) has also been determined for radiotherapy source, as a function of energy (Glaser *et al* 2014); reproduced in Figure 3). The yield increases with photon energy until reaching a plateau around 100 photons/MeV.

Cerenkov photon yield per tissue volume is determined by multiplying radiation dose and the experimentally-determined yield factor (R_E) for either photons or electrons:

$$\begin{aligned} N_{\text{Cerenkov}} \left[\frac{\text{photons}}{\text{cm}^3} \right] \quad = \quad & \text{Dose [Gy]} \quad \times \quad \rho_{\text{tissue}} \left[\frac{\text{g}}{\text{cm}^3} \right] \times 10^{-3} \left[\frac{\text{kg}}{\text{g}} \right] \\ & \times R_E \left[\frac{\text{photons}}{\text{MeV}} \right] \times 6.2 \cdot 10^{12} \left[\frac{\text{MeV}}{\text{J}} \right] \end{aligned} \quad (5)$$

For example, tissue receiving 1 Gy from a 10 MV photon beam $\left(R_E = 85 \text{ photons/MeV}\right)$ would generate 5.3×10^{11} Cerenkov photons per cm^3 of irradiated tissue.

2.3.4 Model of Cerenkov-activated photodynamic therapy—Reported thresholds for effective PDT range from 10^7 to 10^9 $^1O_2$ molecules per cell (Patterson *et al* 1990, Georgakoudi *et al* 1997, Farrell *et al* 1998, Niedre *et al* 2003). We estimated cell killing probability using the lowest reported threshold, $N_{kill} = 4{\times}10^7$ $^1O_2$ molecules per cell, which killed 63% of cells (one log) and was determined *in vitro* using protoporphyrin IX photosensitizer and OCI-AML5 cells (Niedre *et al* 2003).

For the numerical values listed in Table 2, Cerenkov photon yield, radiation dose and probability of cell killing due to PDT effects were estimated under the following optimistic assumptions: 1) the photosensitizer has 100% quantum efficiency at all wavelengths, 2) lowest killing threshold $N_{kill} = 4{\times}10^7$ molecules / 63% cells); 3) cells are 10 μm-radius spheres; and 4) all ROS produced by Cerenkov-PDT are equally potent to $^1O_2$.

The number of $^1O_2$ molecules generated per cell from the excitation of the photosensitizer by Cerenkov light can be computed as:

$$N_{\text{singlet}}\left[\frac{^1O_2}{\text{cell}}\right] = 1\left[\frac{^1O_2}{\text{photon}}\right] \times N_{\text{Cerenkov}}\left[\frac{\text{photons}}{\text{cm}^3}\right] \times \text{cell volume}\left[\text{cm}^3\right] \quad (6)$$

Furthermore, the probability of a single cell being killed by a given dose of singlet oxygen can be approximated by a simple exponential relationship (Weston and Patterson 2008):

$$\text{Prob. of killing single cell} = 1 - \exp\left(-\frac{N_{\text{singlet}}\left[^1O_2 \text{ molecules/cell}\right]}{N_{\text{kill}}\left[^1O_2 \text{ molecules/cell}\right]}\right) \quad (7)$$

2.3.5 Summary of previous results—Reports of CL-activated PDT are summarized in Table 2 (radionuclides) and Table 3 (radiotherapy sources) and include estimations of Cerenkov photon yield, radiation dose, and probability of cell killing due to PDT effects. All extrapolated quantities are determined using methods and equations described in sections 2.3.2 and 2.3.3. The detailed calculations are also provided in a spreadsheet included as Supplemental Information.

For radionuclide sources: The radionuclide was assumed to fully decay, except for long-lived radionuclides such as ^{90}Y, as noted in Table 2; the radiotracer accumulated entirely in the treatment volume (tumor or culture well), the emitted kinetic energy was entirely absorbed in the tumor volume or culture well media volume; cell killing was estimated for *in vivo* tumors by assuming that all photons generated in the tumor volume were absorbed by photosensitizer molecules in the tumor and converted to $^1O_2$ with 100% efficiency; cell killing was estimated for *in vitro* cultures as before, but assuming that 50% of Cerenkov

photons generated passed through a 10 μm cell monolayer and the photosensitizer optical absorption coefficient was $\mu_a = 1\ cm^{-1}$.

For MV photon sources (e.g. linac): Cerenkov photon yield was computed from radiation dose (Gy) to the treatment volume (volume of liquid in culture well); photons absorbed by the cells were computed by assuming all generated photons passed through the 10 μm cell monolayer and the photosensitizer optical absorption coefficient was $\mu_a = 1\ cm^{-1}$; cell killing was estimated by assuming absorbed photons were all converted to $^1O_2$.

For (Kotagiri *et al* 2015), the estimated % of tumor cells killed from Cerenkov-activated PDT is 0.25% per 32 MBq ^{18}FDG injection (assuming that the entire injected dose accumulates in the tumor). The starting volume for HT1080 tumors was ~50 mm^3, and this would constitute an expected reduction of 0.13 mm^3. This estimated therapeutic effect is small compared to the reported tumor suppression of >30 days, compared to untreated controls which grew to volumes >300 mm^3. The corresponding estimated radiation dose to the tumor, assuming 100% of the injected dose in the tumor, is >100 Gy, one that should achieve excellent tumor control.

Additionally, it should be emphasized that cell killing is greatly overestimated in this model and only a small fraction of generated photons will result in production of an ROS molecule. The corresponding estimated radiation dose is 10–100 Gy for most studies examined, a significant one that would be expected to reproductively kill >99% of all cells. This simple model strongly suggests that the biological effects due to Cerenkov activated-PDT should be exceedingly small, even at tumoricidal radiation doses.

Critical analysis of results in both Table 2 and Table 3 reveals a similar trend for all experiments: minimal estimated Cerenkov-PDT-induced cell killing, even at very significant radiation dose levels. Based on these results, we conclude that Cerenkov activation of PDT is not the cause of the observed potent therapeutic effect. Most likely, it is a combination of direct excitation of the photosensitizer by ionizing radiation, physical radiosensitization by dense nanoparticles, and nanoparticle surface catalysis. Additionally, past studies have not always used the most appropriate assays for assessing radiation cell killing *in vitro* (discussed in section 2.3.7) and thus may underestimate the biological effects of ionizing radiation.

Energetic charged particles (created through beta decay or as secondary particles from energetic photons) deposit energy along their path, which can excite photosensitizers through direct excitation and ionization mechanisms (Pratt *et al* 2018). Furthermore, physical radiosensitization occurs when dense, high-Z nanoparticles absorb ionizing radiation and re-emit the absorbed energy in the form of short-range Auger electrons, which are highly damaging to cells due to their high linear energy transfer (T. Butterworth *et al* 2012). Finally, catalysis due to a structured water layer on the nanoparticle surface can weaken H-OH bonds and greatly enhances the efficiency of hydroxyl ($^{\bullet}$OH) production. A 1 nM concentration of 32.5 nm-diameter gold nanoparticles doubles the hydroxyl radical production efficiency (from 200 to 400 nM $^{\bullet}$OH/J) (Sicard-Roselli *et al* 2014).

It must also be noted that *in vitro* cell culture conditions do not appropriately model the optical absorption of Cerenkov light in the medium. Unlike in a tumor, cell culture medium is mostly transparent to visible light, therefore Cerenkov light emitted anywhere within the irradiation volume may propagate to the cell layer at the bottom of the culture vessel. Because of that, the amount of Cerenkov light reaching the cells is strongly dependent upon the volume of medium being irradiated. Furthermore, addition of material in the beam path (such as solid water, as in (Yoon *et al* 2017)), can increase the generation of Cerenkov radiation beyond what would be observed within a tumor.

Finally, photoreactivable DNA damage may also play a role in observed Cerenkov-induced cell killing, though it has not been explored in eukaryotic cells. This type of DNA damage is unique in that it can be repaired by a light-mediated, enzyme-driven process called photoreactivation. Cerenkov luminescence was shown to induce the majority (70%) of photoreactivable DNA damage from ionizing MV photon radiation (Moss and Smith 1980).

2.3.6 Direct ROS production through water radiolysis—These results should be considered in light of the ROS molecules that are produced directly through water radiolysis, the molecular decomposition of water through ionization and excitation mechanisms. Water radiolysis products are e^-_{aq} (solvated electron), $^\bullet OH$ (hydroxyl radical), $H^\bullet$ (hydrogen), $HO_2^\bullet$ (water radical), H_3O^+ (hydronium), ^-OH (hydroxide), H_2O_2 (peroxide), H_2 (dihydrogen), and $^1O_2$ (singlet oxygen – in aerated solutions) (Caër and Sophie 2011, Sharpatyi and Kraljić 1978). Water radiolysis creates 2.7×10^4 $^\bullet OH$ radicals and 1000–3000 $^1O_2$ molecules per MeV of deposited energy (Schwarz 1981, Sharpatyi and Kraljić 1978). Radiolysis-generated $^\bullet OH$ radicals are the primary mechanism of ionizing radiation induced cellular damage (Hall and Giaccia 2011). These yields are substantial when compared to Cerenkov luminescence, which yields no more than 100 photons per MeV of absorbed energy. As a result, the number of ROS molecules created through the direct action of ionizing radiation greatly exceeds the number of bioactive molecules potentially produced by Cerenkov luminescence.

2.3.7 Cell viability assays—The standard for assessing tumor therapy is *clonogenicity*, the capacity of a tumor cell to regenerate indefinitely (Hall and Giaccia 2011). Because the harmful consequences of a tumor stem from its proliferation, this standard is the most relevant from a clinical standpoint. Cancer cells that do not proliferate are not a threat to the patient. The traditional way to assay clonogenicity is the colony formation assay (Franken *et al* 2006), where a known number of cells are plated and the fraction forming colonies (defined to be 50 cells or more) are counted.

Many previous *in vitro* studies have relied on assays such as MTS, MTT, WST-1, and XTT, which reflects the number of metabolically active cells. These assays detect the activity of metabolic enzymes by measuring a colorimetric change brought about by the reduction of tetrazolium salts. Metabolic assays are insensitive to clonogenicity and generally inappropriate for assessing cell survival in the context of radiation treatment. A radiation dose of 10 Gy is considered sufficient to clonogenically kill most mammalian tumor cells, yet most cells would remain metabolically active for some time and appear “viable” using a

metabolic assay; a dose of 100 Gy is required to halt cell functions (e.g. metabolism) (Hall and Giaccia 2011).

3 Scintillation

3.1 Physics

Scintillation has been defined as "luminescence induced by ionizing radiation in transparent, dielectric media" (Lecoq *et al* 2016). The additional characteristics of 1) generation by a scintillator via 2) a series of distinct processes capture how the word has traditionally been used and distinguish it from other phenomena such as Cerenkov radiation. *Scintillators* are the physical materials that facilitate scintillation by transforming absorbed ionizing radiation into lower energy photons (Lecoq *et al* 2016). Scintillators can be inorganic or organic materials.

3.1.1 Inorganic scintillators—Inorganic scintillators are typically single crystals doped with impurities that confer their luminescent properties, but they can also be semi-crystalline (ceramics) or amorphous (glasses). They are made of dense, high-Z materials, which have increased probability of absorbing ionizing radiation through photoelectric interactions. Unlike fluorescence, scintillation is not a property of a single molecule but an emergent bulk property of the inorganic scintillator material.

When ionizing radiation is absorbed by an inorganic scintillator, electrons are excited to the conduction band and leave positively charged holes in the valence band (Figure 4). After a process known as thermalization, these excited electron-hole pairs migrate within the conduction and valence band of the crystal lattice, respectively, and can enter luminescence centers, quenching centers or traps. Luminescence centers are excited when an electron-hole pair (exciton) recombines, and then emit light. Quenching centers can be similarly excited but they relax through non-radiative thermal dissipation. Traps capture and retain electrons or excitons until they return to the conduction band via acquisition of optical or thermal energy or to the valence band via a radiationless transition (Birks 1964).

3.1.2 Organic scintillators—Organic scintillators can be solid (crystal or polymer) or liquid; they can be composed of a single molecule (unary) or a system comprising a solvent and one (binary) or more (ternary, quaternary, etc.) solute molecules that are added to enhance fluorescence (Birks 1964). Organic scintillators, unlike inorganic ones, have scintillation properties that come from individual molecules and not from bulk properties of the material. Liquid and solid organic scintillators luminesce through the same physics: excitation by absorption of radiation, non-radiative Forster resonance transfer of excitation to a fluorophore, and luminescent emission.

Solid organic scintillators can be crystals (e.g. anthracene) or polymers (e.g. polystyrene, polyvinyltoluene) with solute (e.g. p-terphenyl) to enhance luminescence. Typical efficiency for solid organic scintillator is 10^4 photons / MeV (Cherry *et al* 2012).

Liquid scintillators are chemical cocktails composed of an aromatic solvent (such as toluene) and small quantity of dissolved luminophore solute. Ionizing radiation interacts in

the solvent and can yield numerous products (e.g. ions, radicals, excited molecules, fragments, luminescence, x-rays), depending on energy and radiation type. These competing energy- and particle-dependent processes cause luminescent yield from a given energy to be greatest for electrons, then protons, followed by alpha particles. Typical efficiency for a liquid organic scintillator is 10^4 photons / MeV for electrons (Horrocks 1974).

3.2 Applications

3.2.1 Nuclear medicine and x-ray imaging—Bulk inorganic scintillators are a key component of nuclear imaging detectors, surgical gamma probes, X-ray imaging arrays, and well counters. In a nuclear imaging detector, incident gamma or annihilation photons are converted into light by solid inorganic scintillators. Sensitive optical detectors such as photomultiplier tubes or silicon photomultipliers sense the scintillation light, which is proportional to the absorbed photon energy. Typical inorganic scintillators used are: NaI(Tl), CsI(Tl), BGO, LYSO, or LSO. For comprehensive coverage of this topic see (Knoll 2010) and (Cherry *et al* 2012).

Organic scintillators are used in surgical beta probes, radiotherapy dosimeters, and in liquid scintillation counters. For surgical beta probes, they are favored compared to inorganic ones, due to decreased efficiency for gamma photon absorption (Daghighian *et al* 1994). Organic scintillator fibers have been explored as part of monitoring systems for quality assurance and real-time *in vivo* dosimetry (Beddar 2006). Finally, liquid scintillation counters are used for quantification of short-range alpha- or bets-emitting radionuclides, which are difficult to measure by other means (Horrocks 1974).

3.2.2 Radioluminescence microscopy—Radioluminescence microscopy (RLM) is an imaging modality that permits cellular-resolution imaging of beta-emitting radionuclides, which is otherwise not possible with PET or SPECT imaging. It consists of a high sensitivity camera coupled to a microscope objective that images a thin (typically 100–500 μm) $CdWO_4$ scintillator placed above or below a culture monolayer (Kim *et al* 2017). By imaging beta particle scintillation tracks and applying a reconstruction algorithm (Pratx *et al* 2013), <20 μm resolution is achievable (Wang *et al* 2017). RLM has been used to study metabolism (^{18}F-FDG), transgene expression (^{18}F-FHBG) (Pratx *et al* 2012), and cell proliferation with ^{18}F-FLT (Sengupta and Pratx 2016) in MDA-MB-231 human breast adenocarcinoma.

4 Radioluminescent nanoparticles

4.1 Physics

4.1.1 Interaction of tissue and ionizing radiation—The physics governing the interaction of nanoparticles, tissue, and ionizing radiation are depicted in Figure 7. Energetic photons (e.g. X-rays, gamma rays) interact with biological tissues primarily through two effects (Compton scattering and photoelectric absorption) and, by these processes, impart energy to an ejected electron (called recoil electron or photoelectron, respectively).

4.1.2 Interaction of nanoparticles and ionizing radiation—The introduction of high-Z nanoparticles increases the X-ray absorption cross section, particularly at lower energies (<100 keV). The radiation dose in the immediate vicinity of the nanoparticle is enhanced, a phenomenon called physical radiosensitization (T. Butterworth *et al* 2012). However, it important to note that the energy transferred from an X-ray photon to a nanoparticle is for the most part released into the surrounding medium due to the small size of nanoparticles compared to the range of ionizing charged particles. As a result, only a small fraction of the energy of the interacting X-ray is available to stimulate nanoparticle luminescence.

4.1.3 Materials and Physiochemical Properties—Radioluminescent nanoparticles are made of materials that luminesce when excited with ionizing radiation. Attachment of high affinity ligands, such as antibodies, peptides or small molecules, or physiological trafficking of these nanoparticles allow for optical imaging of specific molecular processes. Nanoparticle-based probes have drawn significant attention for their unique physiochemical properties when applied in these biological applications. Novel nanoscintillators, such as quantum dots (Nikolopoulos *et al* 2016), metal nanoclusters (Osakada *et al* 2014), metal organic frameworks (Wang *et al* 2014), and polymer dots (Osakada *et al* 2013) have been examined as radioluminescent probes. However, the most widely studied ones are nanophosphors, which have become synonymous with nanoscintillators. Phosphors are materials that luminesce in the form of either fluorescence or phosphorescence when excited with radiation. They are prevalent in the biomedical field in X-ray screens (Yaffe and Rowlands 1997) and, more recently, as contrast agents for X-ray luminescence imaging.

A unique feature of nanomaterials, including nanoscintillators, is their high surface area-to-volume ratio, which allows for extensive surface loading and potential multivalent binding to facilitate specificity. The role of the surface chemistry also has a significant impact on the biological interaction of the nanoparticle in the bloodstream for *in vivo* applications. Biocompatible coatings are necessary to avoid rapid clearance by the immune system; however, these may also affect energy transfer in PDT applications in which photosensitizers are grafted via linker molecules. Another important consideration is the surface of the nanocrystals, as these sites and defects may negatively impact the luminescent output of the material in comparison to their bulk properties (Dujardin *et al* 2010). To address this potential surface quenching, nanophosphors comprised of core-shell architectures have been employed to improve radioluminescence efficiency (Naczynski *et al* 2015).

4.2 Applications

4.2.1 Radioluminescent nanoparticle imaging—Tomographic radioluminescence imaging modalities are inspired from *fluorescence x-ray computed tomography* (XFCT; (Cesareo and Mascarenhas 1989), a method that forms images by exciting and detecting X-ray fluorescence. However, unlike XFCT, they form images by detecting optical, rather than X-ray, photons.

X-ray luminescence computed tomography (XLCT) uses an X-ray pencil beam to excite nanophosphor contrast agents, which emit near-infrared (NIR) photons that are detected with

an optical detector. The approach takes advantage of weak scattering in tissue of the X-ray excitation beam and enables reconstruction of high quality, tomographic images regardless of optical scatter (Pratx *et al* 2010a, 2010b, Li *et al* 2013).

A critical factor in the development of these imaging platforms is the uptake or total quantity of materials accumulating at sites of interest. Few studies have demonstrated target-specific accumulation of probes with subsequent *in vivo* imaging. Often, concentrations administered via intravenous injection are close to the limit of detection. However, depending on the imaging application (e.g. tumor cell detection), the accumulation of probes can increase if preferential uptake by target cells is achieved. An additional factor to consider is the local aggregation of the material in endosomal and lysosomal compartments, which could impact local nanoparticle densities and subsequent energy transfer between different excited nanoparticles. Unique applications of X-ray luminescence imaging include cancer cell imaging in the 1000–1500 nm window (Naczynski *et al* 2015), pH monitoring (Chen *et al* 2013), and drug delivery (Moore Thomas L. *et al* 2014).

4.2.2 X-ray activated photodynamic therapy—There is growing interest in combining nanoparticle scintillators with radiotherapy to activate photodynamic therapy (Morgan *et al* 2009, Scaffidi *et al* 2011, Chen *et al* 2015, Clement *et al* 2016). The general reasoning is that these nanoparticles will efficiently transduce X-ray energy into light for photosensitizer activation and thereby provide additional efficacy during radiotherapy with no additional radiation dose.

In vitro evidence of nanoparticle efficacy has been reported using psoralen-conjugated Y_2O_3 nanoparticles (Scaffidi *et al* 2011). However, the reported biological effect is small, with physical radiosensitization, due to the presence of nanoscintillator alone, being the dominant factor. X-ray-activated PDT has also been tested *in vitro* using 8 keV X-rays and a CeF_3 nanoparticle conjugated to vetereporfin (Clement *et al* 2016). This low energy used in this experiment is favorable for observing an effect, due to the greatly enhanced X-ray absorption cross-section of the nanoparticle, yet low energy X-rays are not practical for radiotherapy. In the following Models section, we review the theoretical basis for this idea and provide an appropriate model for estimating its efficacy.

4.2.3 Clinical evidence of PDT-activation through non-light mechanism—Therapeutic enhancement has been reported by combining a photosensitizer with radiotherapy; significant necrosis and inhibition of mouse osteosarcoma tumors, compared with sham-treated mice, was reported using a 5 Gy dose and acridine orange photosensitizer (Hashiguchi *et al* 2002). A subsequent uncontrolled clinical trial treated six synovial sarcoma patients with a 5 Gy radiotherapy beam dose and acradine orange and none had local recurrence during follow up (ranged from 19–52 months) (Kusuzaki *et al* 2005). A semi-controlled study found better outcomes with minimally invasive surgery followed by radiotherapy and acridine orange, than wide limb resection alone (Matsubara *et al* 2010). None of these studies was rigorously controlled so as to generate the highest level of medical evidence. However, their consistency and results are encouraging and suggest the possibility of a non-light-based mechanism of PDT activation.

4.3 Models

4.3.1 Limitations of previous models—Previous studies have theoretically investigated the use of nanoparticles to transduce ionizing radiation into optical photons for activation of PDT (Morgan *et al* 2009, Clement *et al* 2016). Based on the assumption that X-ray photons impinging on a nanoparticle would transfer all of their energy to that nanoparticle, these studies have concluded that this strategy would be effective for photon sources <300 kV.

An alternative model for nanoscintillator-mediated PDT recognizes that secondary electrons generated in the nanoscintillator have ranges much greater than the size of the nanoscintillator (Bulin *et al* 2015). Therefore, contrary to prior assumptions, only a small fraction of the X-ray energy will generate light within the nanoscintillator. At physiological nanoparticle concentrations (i.e. <1 mg/cm^3), biological effects of radiation are primarily mediated by water, the most abundant molecule in biological tissues. Upon absorbing X-ray photons, water releases energetic electrons (mostly Compton recoil electrons) that propagate through the tissue and deposit energy along their path. When such an electron encounters a nanoparticle, some of its energy is transferred to the nanoparticle, stimulating the emission of light (Figure 7). The amount of energy transferred is a function of the electron energy, nanoparticle size, and nanoparticle composition (electron stopping power and density; (Berger *et al* 2005). The typical energy transfer between an electron and 20 nm diameter nanoparticle is on the order of 10 eV. This indirect transfer of energy from ionizing photon to scintillator molecule is the primary mechanism for X-ray luminescence.

4.3.2 Proposed electron absorption cross section-based model—Because X-ray are predominantly absorbed by water molecules, the efficiency of X-ray luminescence is nearly independent of nanoparticle X-ray stopping power. The luminescence yield can be approximated as a function of the radiation dose to tissue (unit: Gy), the nanoparticle mass concentration C_{NP} (unit: g/cm^3), the scintillator light yield Y_{sc} (assumed here to be 10^5 photons/MeV) and the electron cross-sections (μ/ρ) for tissue and the nanoparticle material. The modified model for estimating the density of scintillation photons emitted by the nanoparticle is:

$$N_{\text{scint}}\left[\frac{\text{photons}}{\text{cm}^3}\right] = \text{Dose}\left[\frac{\text{J}}{\text{kg}}\right] \times 10^{-3}\left[\frac{\text{kg}}{\text{g}}\right] \times 6.2 \times 10^{12}\left[\frac{\text{MeV}}{\text{J}}\right] \times C_{NP}\left[\frac{\text{g}}{\text{cm}^3}\right] \times \frac{\left(\mu/\rho\right)_{\text{NP}}\left[\text{MeV}\cdot\text{cm}^2/\text{g}\right]}{\left(\mu/\rho\right)_{\text{tissue}}\left[\text{MeV}\cdot\text{cm}^2/\text{g}\right]} \times Y_{\text{sc}}\left[\frac{\text{photons}}{\text{MeV}}\right] \quad (8)$$

A derivation of this equation is provided as Online Supplemental Information. The stopping power coefficients for electrons (μ/ρ) can be obtained from the ESTAR database, which is maintained by the National Institute of Standards and Technologies (NIST). Singlet oxygen concentration $\left(C_{1o_2}\right)$ is calculated by assuming that all photons are converted to singlet oxygen molecules:

$$C_{^1O_2}\left[\frac{^1O_2 \text{ molecules}}{\text{cm}^3}\right] = N_{\text{scint}}\left[\frac{\text{photons}}{\text{cm}^3}\right] \times 1\left[\frac{^1O_2 \text{ molecules}}{\text{photons}}\right] \quad (9)$$

The number of singlet oxygen molecules per cell $\left(N_{1o_2}\right)$ is calculated using the cell volume estimated assuming 10 μm diameter spherical cells:

$$N_{^1O_2}\left[\frac{^1O_2 \text{ molecules}}{\text{cell}}\right] = C_{^1O_2}\left[\frac{^1O_2 \text{ molecules}}{\text{cm}^3}\right] \times 4.2 \times 10^{-9}\left[\frac{\text{cm}^3}{\text{cell}}\right] \quad (10)$$

The model based on electron stopping power should more accurately predict the efficacy of X-ray PDT, compared to previous models. It should be effective for predicting PDT efficacy within the correct order of magnitude. However, it should be noted that values obtained with this model represent an upper bound for the actual number of scintillation photons emitted, as explained in the supplemental information, and thus are approximate. The model also does not account for enhanced radiation dose (physical radiosensitization) near nanoparticles, and therefore it is valid mainly for low nanoparticle concentrations (< 10 mg/cm^3), where particles are relatively far from one another. For greater accuracy, Monte Carlo simulations, which model photon-nanoscintillator interactions in greater detail, are necessary (Bulin *et al* 2015).

Sample photon yields are computed in Table 4 for 1 Gy radiation delivered to tissue containing 1 mg/cm^3 LaF_3 nanoscintillator. Over a large energy range, photon production by the nanoscintillator is relatively inefficient, yielding <100 photons per MeV of energy deposited. Although less efficient than Cerenkov luminescence, nanoparticle radioluminescence is localized to the nanoparticle, and therefore the scintillation light may be easier to harvest for efficient photosensitizer excitation. These calculations are also provided in a convenient spreadsheet included as Supplemental Information.

The table also shows that LaF_3 (and other high-Z materials) have a lower mass-energy attenuation coefficient (μ/ρ) for electrons than water. This reflects the fact that the nucleus of high-Z atoms contains a higher fraction of neutrons than protons, compared to lower-Z nuclei. Nevertheless, the high density of nanoparticles ultimately results in increased absorption cross-section and enhanced energy absorption compared to water.

4.3.3 Comparison of proposed electron cross section model with previous photon-based model—

The impact of electron cross sections can be demonstrated by substituting electron for photon cross sections into the model that predicts singlet oxygen molecules per cell (Morgan *et al* 2009). Here, the volume of a cell is taken to be 4.2×10^{-9} cm^3 (10 μm-diameter sphere) and a concentration of 3 mg/cm^3 of LaF_3 NP is assumed. The modified model predicts ~10^6 $^1O_2$ per cell over a wide energy range and is factor of 10^1 to 10^3 less than the original model (Figure 8). This result is much less than the needed 10^7 $^1O_2$

per cell PDT threshold (Niedre *et al* 2003) and suggests that even a 60 Gy dose would be insufficient for an enhancement effect.

5 Air fluorescence

5.1 Physics

Air fluorescence, also known as *air scintillation*, is fluorescence emitted by atmospheric gases excited and/or ionized by radiation. The three most abundant atmospheric gases—nitrogen (78% v/v), oxygen (21% v/v) and argon (1% v/v)—determine the fluorescent yield. Other atmospheric gases such as CO_2 and CH_4 are potent fluorescent quenchers (Morii *et al* 2004), but not present in quantities (US EPA 2016) sufficient to appreciably influence fluorescent yield.

Nitrogen fluoresces primarily via $N_2 \rightarrow N_2^*$, $N_2 \rightarrow {N_2}^{+*}$, or $N_2 \rightarrow {N_2}^{+*}$ (where * denotes an excited state and $^+$ denotes positive charge due electron loss) reactions which yield of 141 photon/MeV of deposited energy (Morii *et al* 2004). Argon fluoresces brightly, yielding 10^4 photon/MeV via primary $Ar \rightarrow Ar^*$ (Suzuki and Kubota 1979) and secondary three-body: $Ar^* + 2Ar \rightarrow {Ar_2}^* + Ar$, ${Ar_2}^* \rightarrow 2Ar + \text{photon}$ reactions (Monteiro *et al* 2008). Oxygen is weakly fluorescent, yielding ~0.5 photons/MeV of deposited energy (Morii *et al* 2004), yet it is also a powerful quencher of nitrogen and argon fluorescence via ${N_2}^* + O_2 \rightarrow N_2 + {O_2}^*$ and $Ar^* + O_2 \rightarrow Ar + {O_2}^*$ reactions. Consequently, the spectral properties of air fluorescence are dominated by nitrogen while the fluorescent yield, 25 photons/MeV deposited energy, is dominated by the quenching action of oxygen.

5.2 Applications

Air fluorescence has been used to detect the interaction of high-energy cosmic radiation with the Earth's upper atmosphere, which produce an abundance of secondary radiations dispersed over hundreds of square kilometers.

Air fluorescence can be imaged during radiotherapy, providing monitoring capabilities that could prevent gross dosimetry errors during treatment (Fahimian *et al* 2014). This approach is relatively simple to implement and would consist of a sensitive camera optimized for ultraviolet imaging and short-pass filters to block ambient room lighting; gating image acquisition with radiotherapy source pulse could also greatly improve signal-to-noise ratio.

Air fluorescence can be a significant source of background during X-ray luminescence imaging, especially in the kV range. Fortunately, this emission is primarily at wavelengths below 430 nm, thus it can be blocked using a suitable long-pass filter.

5.3 Models

5.3.1 Air fluorescence yield from typical radiotherapy source—Air fluorescence yield from a radiotherapy source is estimated at a point along the beam as follows. The considered geometry is depicted in Figure 11.

Dose to air is the related to dose to water according to the ratio of their respective mass attenuation coefficients. Furthermore, if we assume that luminescence is observed at a distance r from the source and that dose to water is for a given source-to-surface distance (SSD; r<SSD; Figure 11), the divergence of the beam emanating from the linear accelerator can be modeled by incorporating a $1/r^2$ factor into the formula:

$$\text{Dose}_{\text{air}}\,[\text{Gy}] = \left(\frac{\text{SSD}\,[\text{cm}]}{r\,[\text{cm}]}\right)^2 \times \frac{(\mu/\rho)_{\text{air}}\left[\text{cm}^2/\text{g} \text{ or } \text{MeV}\cdot\text{cm}^2/\text{g}\right]}{(\mu/\rho)_{\text{tissue}}\left[\text{cm}^2/\text{g} \text{ or } \text{MeV}\cdot\text{cm}^2/\text{g}\right]} \times \text{Dose}_{\text{tissue}}\,[\text{Gy}] \quad (11)$$

The energy deposited in air (MeV/cm^3) is computed by multiplying the dose by air density ($\rho_{\text{air}} = 1.23\cdot10^{-6}$ kg/cm^3) and MeV per joule unit conversion factor:

$$\text{Energy deposited}_{\text{air}}\left[\frac{\text{MeV}}{\text{cm}^3}\right] = \text{Dose}_{\text{air}}\left[\frac{\text{J}}{\text{kg}}\right] \times \rho_{\text{air}}\left[\frac{\text{kg}}{\text{cm}^3}\right] \times\ 6.242 \times 10^{12}\left[\frac{\text{MeV}}{\text{J}}\right] \quad (12)$$

Finally, light production (photons/cm^3) is determined by multiplying the deposited energy by experimentally-determined air fluorescence yield (Morii *et al* 2004):

$$\Phi\ \left[\frac{\text{photons}}{\text{cm}^3}\right] = \text{Energy deposited}_{\text{air}}\left[\frac{\text{MeV}}{\text{cm}^3}\right] \times 25\ \left[\frac{\text{photons}}{\text{MeV}}\right] \quad (13)$$

Estimated photon yield for electron and photon sources of typical radiotherapy energies are listed in Table 5, assuming 1 Gy to tissue at SSD = 100 cm. Mass-energy attenuation coefficients for photon and electrons in air and tissue were sourced from online databases (Berger *et al* 2005, 2009). The calculations are also provided in a spreadsheet included as Supplemental Information.

6 Persistent/delayed luminescence

6.1 Physics

Persistent luminescence is a phenomenon that is caused by slow liberation of radiation-induced trapped charged carriers (Van den Eeckhout *et al* 2010). *Thermoluminescence* is the heating of persistent luminescent materials to liberate radiation-induced electrons that were trapped at metastable sites. Luminescence is produced when these electrons recombine with corresponding holes and is used to reveal trap levels in a given material (Van den Eeckhout *et al* 2010). *Optically-stimulated luminescence*, similar to thermoluminescence, is optically induced liberation of trapped electrons. These electrons similarly recombine with localized holes, producing luminescence (Boetter-Jensen *et al* 2003). The emitted luminescence is proportional to radiation dose accumulated by the material (Nelson *et al* 1967), a useful relationship that has been used for dating of archaeological and geological materials, biological dosimetry, and in photostimulable phosphor plates used for X-ray medical imaging (Rowlands 2002).

In the *in vivo* setting, detectable in irradiated animals and persisting for minutes following irradiation, this phenomenon has been called *radiobioluminescence* (Rao 2015). This effect has been observed both in live and dead tissues, suggesting that its origin is not biological but physical. The mechanism is likely related to food thermoluminescence, caused by presence of thermoluminescent minerals (e.g. sand and dust; (Sanderson *et al* 1989, Soika and Delincée 2000).

6.2 Applications

Persistent luminescent nanoparticles, both silicate- and polymer-based, have been developed for preclinical imaging and *in vivo* PDT activation. They have favorable properties for sensitive *in vivo* imaging (Chermont *et al* 2007, Maldiney *et al* 2012, Palner *et al* 2015). These are: 1) can be excited with visible, ultraviolet, or x-ray photons before administration or *in vivo*, repeatedly; 2) emission wavelengths in the 600–800 nm range, which is favorable for imaging owing to weak attenuation by biological tissues; 3) can luminescence for >10 hours (Maldiney *et al* 2013), eliminating background signal induced by excitation source (*e.g.* autofluorescence).

Persistent luminescence nanoparticles have been developed that can be repeatedly excited *in vivo* by external X-ray irradiation for imaging and activation of PDT (Chen *et al* 2017, Song Liang *et al* 2018), as shown in Figure 13.

7 Radioluminescence of biologically-endogenous molecules

7.1 Physics

7.1.1 Protein and amino acid luminescence—Biological molecules such as trypsin, tyrosine, phenyalanine, and tryptophan exhibit both immediate luminescence and long afterglow following X-ray irradiation. Immediate luminescence emitted is fluorescence caused by electron excitation; it decreases with absorbed dose likely due to temporary molecular damage (Nelson *et al* 1967).

7.1.2 Water radioluminescence—Radioluminescence has been observed in pure water (Sitharamarao and Duncan 1963) at energies below the Cerenkov threshold (Quickenden 1971, Tarasov *et al* 2007, Spinelli *et al* 2011, Yamamoto *et al* 2016). Mechanisms for experimentally-observed water radioluminescence are fluorescence and chemiluminescence related to trace impurities as well as fluorescence of water and radiolysis products.

Impurity-related luminescence can be caused by direct excitation of endogenous luminophores dissolved in water (e.g. aromatic amino acids, humic compounds; (Belovolova *et al* 2009) or chemiluminescence resulting from the reaction of water radiolysis products with trace impurities (Vasil'ev, R.F. 1970). Impurity-related luminescence is not observed in purified water.

Water is inherently fluorescent (Quickenden 1971, Belovolova *et al* 2009) and water-radiolysis products, including hydroxyl radicals ($^{\bullet}OH$), singlet oxygen ($^1O_2$), hydrated electrons (e_{aq}^-) are also fluorescent (Sitharamarao and Duncan 1963, Quickenden 1971).

Water radioluminescence is ~60× less efficient than air fluorescence, equating to a yield of <1 photon/MeV of deposited energy (Tarasov *et al* 2007).

7.2 Models

Similar to air fluorescence (see section 5.3), the radioluminescence of biological molecules is proportional to the energy deposited into them.

7.3 Applications

Water radioluminescence, used in combination with a water phantom and sensitive camera, has been suggested as a means of dose estimation for lower energy x-ray beams (Yamamoto *et al* 2016). It could supplement or replace ionization chamber point measurements. Compared to Cerenkov luminescence, the signal is not hampered by threshold effects. It could also be used to measure the range of protons and ion beams in water, given that these particles do not generate Cerenkov luminescence at clinically relevant energies (Yamamoto *et al* 2016).

Endogenous radioluminophores such as aromatic amino acids (e.g. tryptophan) can also be imaged with XLCT, using suitable emission filters. However, in most situations, they create an unwanted luminescent background that impede the detection of low concentrations of administered molecular probes. Spectral or temporal filtering approaches must be implemented to reject this “auto-radioluminescence” and achieve high sensitivity with XLCT.

8 Summary

8.1 Summary of radioluminescence sources

Radioluminescence has been explored for a multitude of biomedical applications and this review has endeavored to summarize the physics and applications of all relevant phenomena. We note a recent and complementary review that focuses on biomedical applications at the intersection of optical and ionizing radiation (Pogue and Wilson 2018). This summary quantitatively tabulates the strength of each phenomenon in Table 6 and speculates on their utility for either imaging or therapy in the biomedical setting.

8.1.1 Imaging—Single-photon-sensitivity cameras can image all radioluminescence signals, given sufficient integration time. However, some phenomena are impractically weak to be useful in the biomedical setting, especially where better methods are already available.

Scintillator-based detectors have proven their utility for radionuclide and radiological imaging, owing to their ability to efficiently transduce ionizing photons into detectable optical ones. Though advances in scintillator materials and optical detectors have improved their performance over past decades, the general concept has changed little. Recently, scintillators have found new uses as *in vivo* **nanoscintillator** contrast agents for **x-ray luminescence computed tomography** and in **radioluminescence microscopy** for cellular-resolution imaging of beta-emitting radiotracers.

Cerenkov luminescence provides a means for simple, direct imaging of radionuclides via optical signals. It is a suitable substitute for *in vivo* PET imaging when the trade-off of decreased *in vivo* imaging resolution, lack of penetration and absolute quantitation are minor compared to benefits of cost, speed and simplicity. Consequently, preclinical, radiotherapy, and surgical applications appear to be most useful for CLI.

Persistent luminescence has been harnessed extensively in radiation dosimetry and in storage phosphors for X-ray medical imaging. It is also a source of noise emitted by biologically-endogenous molecules during sensitive, prolonged imaging of living organisms. Recently, persistent luminescence nanoparticles have been used for *in vivo* imaging. These materials can be repeatedly excited *in vivo* via X-ray radiation and luminesce for a sustained duration.

Water radioluminescence is the weakest form of radioluminescence. It has been explored for radiotherapy applications, however other methods could likely accomplish the same goal. For example, direct excitation of a fluorescent solution could provide a brighter, more readily detectable signal for kV X-ray dosimetry.

8.1.2 Therapy—Clinical phototherapies require bright, sustained sources of light. Most radioluminescence sources are too weak to provide sufficient radiant exposure to activate these therapies. Our analysis shows that radionuclide-generated **Cerenkov luminescence** is too weak to activate photodynamic therapy at reasonable radioactivity concentrations. Radiotherapy-generated **Cerenkov luminescence** is brighter, but still unlikely as a means of activating phototherapy.

Nanoscintillators have been suggested as therapeutic agents to efficiently transduce radiotherapy photons into light for phototherapy. While these high-Z nanoparticles are certainty effective physical radiosensitizers, our analysis shows their potential contributions to therapy to be exceedingly small at physiological concentrations.

For both Cerenkov luminescence and radiation-activated nanoscintillators, the delivered radiation dose must exceed tumoricidal levels to observe even the smallest PDT effect. We conclude that therapeutic uses of radioluminescence, based on available literature, are unlikely with current nanoparticles and photosensitizers.

Supplementary Material

Refer to Web version on PubMed Central for supplementary material.

Acknowledgments

Justin Klein is a Stanford Molecular Imaging Scholar under NIH grant T32 CA1186810. Conroy Sun acknowledges support from NIH Grant 5R35GM119839. Guillem Pratx receives support from NIH under grants 5R01CA186275 and 5R21CA193001.

References

Ackerman NL and Graves EE 2012 The potential for Cerenkov luminescence imaging of alpha-emitting radionuclides Phys. Med. Biol 57 771 [PubMed: 22252144]

Beattie BJ, Thorek DLJ, Schmidtlein CR, Pentlow KS, Humm JL and Hielscher AH 2012 Quantitative Modeling of Cerenkov Light Production Efficiency from Medical Radionuclides PLOS ONE 7 e31402 [PubMed: 22363636]

Beddar AS 2006 Plastic scintillation dosimetry and its application to radiotherapy Radiat. Meas 41 S124–33

Belovolova LV, Glushkov MV, Vinogradov EA, Babintsev VA and Golovanov VI 2009 Ultraviolet fluorescence of water and highly diluted aqueous media Phys. Wave Phenom 17 21–31

Berger MJ, Coursey JS, Zucker MA and Chang J 2005 NIST Stopping-Power and Range Tables: Electrons, Protons, Helium Ions Online: http://www.nist.gov/pml/data/star/index.cfm

Berger MJ, Hubbell JH, Seltzer SM, Chang J, Coursey JS, Sukumar R, Zucker DS and Olsen K 2009 XCOM: Photon Cross Section Database (version 1.5). [Online] NIST Stand. Ref. Database 8 XGAM Online: https://www.nist.gov/pml/xcom-photon-cross-sections-database

Birks JB 1964 The Theory and Practice of Scintillation Counting: International Series of Monographs in Electronics and Instrumentation (Elsevier)

Boetter-Jensen L, McKeever SWS and Wintle AG 2003 Optically Stimulated Luminescence Dosimetry (Elsevier)

Brunner SE and Schaart DR 2017 BGO as a hybrid scintillator / Cherenkov radiator for cost-effective time-of-flight PET Phys. Med. Biol 62 4421 [PubMed: 28358722]

Bulin A-L, Vasil'ev A, Belsky A, Amans D, Ledoux G and Dujardin C 2015 Modelling energy deposition in nanoscintillators to predict the efficiency of the X-ray-induced photodynamic effect Nanoscale 7 5744–51 [PubMed: 25746211]

Caër L and Sophie 2011 Water Radiolysis: Influence of Oxide Surfaces on H2 Production under Ionizing Radiation Water 3 235–53

Carpenter CM, Ma X, Liu H, Sun C, Pratx G, Wang J, Gambhir SS, Xing L and Cheng Z 2014 Cerenkov Luminescence Endoscopy: Improved Molecular Sensitivity with β−-Emitting Radiotracers J. Nucl. Med 55 1905–9 [PubMed: 25300598]

Cesareo R and Mascarenhas S 1989 A new tomographic device based on the detection of fluorescent x-rays Nucl. Instrum. Methods Phys. Res. Sect. Accel. Spectrometers Detect. Assoc. Equip 277 669–72

Chen H, Moore T, Qi B, Colvin DC, Jelen EK, Hitchcock DA, He J, Mefford OT, Gore JC, Alexis F and Anker JN 2013 Monitoring pH-Triggered Drug Release from Radioluminescent Nanocapsules with X-ray Excited Optical Luminescence ACS Nano 7 1178–87 [PubMed: 23281651]

Chen H, Sun X, Wang GD, Nagata K, Hao Z, Wang A, Li Z, Xie J and Shen B 2017 LiGa5O8:Cr-based theranostic nanoparticles for imaging-guided X-ray induced photodynamic therapy of deep-seated tumors Mater. Horiz 4 1092–101

Chen H, Wang GD, Chuang Y-J, Zhen Z, Chen X, Biddinger P, Hao Z, Liu F, Shen B, Pan Z and Xie J 2015 Nanoscintillator-Mediated X-ray Inducible Photodynamic Therapy for In Vivo Cancer Treatment Nano Lett 15 2249–56 [PubMed: 25756781]

Chermont Q le M de, Chanéac C, Seguin J, Pellé F, Maîtrejean S, Jolivet J-P, Gourier D, Bessodes M and Scherman D 2007 Nanoprobes with near-infrared persistent luminescence for in vivo imaging Proc. Natl. Acad. Sci 104 9266–71 [PubMed: 17517614]

Cherry SR, Sorenson JA and Phelps ME 2012 Physics in Nuclear Medicine (Fourth Edition) Physics in Nuclear Medicine (Fourth Edition) (Philadelphia: W.B. Saunders) pp 63–85 Online: http://www.sciencedirect.com/science/article/pii/B978141605198500006X

Ciarrocchi E and Belcari N 2017 Cerenkov luminescence imaging: physics principles and potential applications in biomedical sciences EJNMMI Phys 4 14 [PubMed: 28283990]

Clement S, Deng W, Camilleri E, Wilson BC and Goldys EM 2016 X-ray induced singlet oxygen generation by nanoparticle-photosensitizer conjugates for photodynamic therapy: determination of singlet oxygen quantum yield Sci. Rep 6 srep19954

Daghighian F, Mazziotta JC, Hoffman EJ, Shenderov P, Eshaghian B, Siegel S and Phelps ME 1994 Intraoperative beta probe: A device for detecting tissue labeled with positron or electron emitting isotopes during surgery Med. Phys 21 153–7 [PubMed: 8164582]

Dothager RS, Goiffon RJ, Jackson E, Harpstrite S and Piwnica-Worms D 2010 Cerenkov Radiation Energy Transfer (CRET) Imaging: A Novel Method for Optical Imaging of PET Isotopes in Biological Systems PLOS ONE 5 e13300 [PubMed: 20949021]

Dougherty TJ, Gomer CJ, Henderson BW, Jori G, Kessel D, Korbelik M, Moan J and Peng Q 1998 Photodynamic Therapy J. Natl. Cancer Inst 90 889–905 [PubMed: 9637138]

Dujardin C, Amans D, Belsky A, Chaput F, Ledoux G and Pillonnet A 2010 Luminescence and Scintillation Properties at the Nanoscale IEEE Trans. Nucl. Sci 57 1348–54

Fahimian B, Ceballos A, Türkcan S, Kapp DS and Pratx G 2014 Seeing the invisible: Direct visualization of therapeutic radiation beams using air scintillation Med. Phys 41 010702 [PubMed: 24387491]

Farrell TJ, Wilson BC, Patterson MS and Olivo MC 1998 Comparison of the In Vivo Photodynamic Threshold Dose for Photofrin, Mono- and Tetrasulfonated Aluminum Phthalocyanine Using a Rat Liver Model Photochem. Photobiol 68 394–9 [PubMed: 9747595]

Franken NAP, Rodermond HM, Stap J, Haveman J and van Bree C 2006 Clonogenic assay of cells in vitro Nat. Protoc 1 2315–9 [PubMed: 17406473]

Georgakoudi I, Nichols MG and Foster TH 1997 The Mechanism of Photofrin Photobleaching and Its Consequences for Photodynamic Dosimetry Photochem. Photobiol 65 135–44 [PubMed: 9066293]

Gill RK, Mitchell GS and Cherry SR 2015 Computed Cerenkov luminescence yields for radionuclides used in biology and medicine Phys. Med. Biol 60 4263–80 [PubMed: 25973972]

Glaser AK, Davis SC, McClatchy DM, Zhang R, Pogue BW and Gladstone DJ 2013a Projection imaging of photon beams by the Čerenkov effect Med. Phys 40 012101 [PubMed: 23298103]

Glaser AK, Davis SC, Voigt WHA, Zhang R, Pogue BW and Gladstone DJ 2013b Projection imaging of photon beams using Čerenkov-excited fluorescence Phys. Med. Biol 58 601 [PubMed: 23318469]

Glaser AK, Zhang R, Andreozzi JM, Gladstone DJ and Pogue BW 2015 Cherenkov radiation fluence estimates in tissue for molecular imaging and therapy applications Phys. Med. Biol 60 6701–18 [PubMed: 26270125]

Glaser AK, Zhang R, Gladstone DJ and Pogue BW 2014 Optical dosimetry of radiotherapy beams using Cherenkov radiation: the relationship between light emission and dose Phys. Med. Biol 59 3789 [PubMed: 24938928]

Grimm J 2015 Cerenkov Luminescence Imaging Imaging and Visualization in The Modern Operating Room ed Fong Y, Giulianotti PC, Lewis J, Koerkamp BG and Reiner T (Springer New York) pp 107–20 Online: http://link.springer.com/chapter/10.1007/978-1-4939-2326-7_8

Grootendorst MR, Cariati M, Kothari A, Tuch DS and Purushotham A 2016a Cerenkov luminescence imaging (CLI) for image-guided cancer surgery Clin. Transl. Imaging 4 353–66 [PubMed: 27738626]

Grootendorst MR, Cariati M, Pinder S, Kothari A, Douek M, Kovacs T, Hamed H, Pawa A, Nimmo F, Owen J, Ramalingam V, Sethi S, Mistry S, Vyas K, Tuch D, Britten A, Hemelrijck MV, Cook G, Sibley-Allen C, Allen S and Purushotham A 2016b Intraoperative Assessment of Tumor Resection Margins in Breast-Conserving Surgery using 18F-FDG Cerenkov Luminescence Imaging – A First-in-Human Feasibility Study J. Nucl. Med. jnumed 116181032

Hall EJ and Giaccia AJ 2011 Radiobiology for the Radiologist (Philadelphia, United States STATES: Wolters Kluwer Health) Online: http://ebookcentral.proquest.com/lib/stanford-ebooks/detail.action?docID=2031840

Hartl BA, Hirschberg H, Marcu L and Cherry SR 2016 Activating Photodynamic Therapy in vitro with Cerenkov Radiation Generated from Yttrium-90 J. Environ. Pathol. Toxicol. Oncol 35 185–92 [PubMed: 27481495]

Hashiguchi S, Kusuzaki K, Murata H, Takeshita H, Hashiba M, Nishimura T, Ashihara T and Hirasawa Y 2002 Acridine Orange Excited by Low-Dose Radiation Has a Strong Cytocidal Effect on Mouse Osteosarcoma Oncology 62 85–93 [PubMed: 11810048]

Helo Y, Rosenberg I, D'Souza D, MacDonald L, Speller R, Royle G and Gibson A 2014 Imaging Cerenkov emission as a quality assurance tool in electron radiotherapy Phys. Med. Biol 59 1963 [PubMed: 24694567]

Horrocks DL 1974 Applications of Liquid Scintillation Counting Applications of Liquid Scintillation Counting (Academic Press) p xiii Online: http://www.sciencedirect.com/science/article/pii/B9780123562401500056

Hu H, Cao X, Kang F, Wang M, Lin Y, Liu M, Li S, Yao L, Liang J, Liang J, Nie Y, Chen X, Wang J and Wu K 2015 Feasibility study of novel endoscopic Cerenkov luminescence imaging system in detecting and quantifying gastrointestinal disease: first human results Eur. Radiol 25 1814–22 [PubMed: 25577521]

Jarvis LA, Zhang R, Gladstone DJ, Jiang S, Hitchcock W, Friedman OD, Glaser AK, Jermyn M and Pogue BW 2014 Cherenkov Video Imaging Allows for the First Visualization of Radiation Therapy in Real Time Int. J. Radiat. Oncol 89 615–22

Jelley JV 1958 Cerenkov Radiation and Its Applications (Pergamon Press)

Kamkaew A, Cheng L, Goel S, Valdovinos HF, Barnhart TE, Liu Z and Cai W 2016 Cerenkov Radiation Induced Photodynamic Therapy Using Chlorin e6-Loaded Hollow Mesoporous Silica Nanoparticles ACS Appl. Mater. Interfaces 8 26630–7 [PubMed: 27657487]

Kim TJ, Türkcan S and Pratx G 2017 Modular low-light microscope for imaging cellular bioluminescence and radioluminescence Nat. Protoc 12 1055–76 [PubMed: 28426025]

Klein JS, Mitchell GS and Cherry SR 2017 Quantitative assessment of Cerenkov luminescence for radioguided brain tumor resection surgery Phys. Med. Biol 62 4183 [PubMed: 28287074]

Knoll GF 2010 Radiation Detection and Measurement (John Wiley & Sons)

Korpar S, Dolenec R, Križan P, Pestotnik R and Stanovnik A 2011 Study of TOF PET using Cherenkov light Nucl. Instrum. Methods Phys. Res. Sect. Accel. Spectrometers Detect. Assoc. Equip 654 532–8

Kotagiri N, Sudlow GP, Akers WJ and Achilefu S 2015 Breaking the depth dependency of phototherapy with Cerenkov radiation and low-radiance-responsive nanophotosensitizers Nat. Nanotechnol 10 370–9 [PubMed: 25751304]

Kusuzaki K, Murata H, Matsubara T, Miyazaki S, Shintani K, Seto M, Matsumine A, Hosoi H, Sugimoto T and Uchida A 2005 Clinical Outcome of a Novel Photodynamic Therapy Technique Using Acridine Orange for Synovial Sarcomas Photochem. Photobiol 81 705–9 [PubMed: 15686440]

Kwon SI, Gola A, Ferri A, Piemonte C and Cherry SR 2016 Bismuth germanate coupled to near ultraviolet silicon photomultipliers for time-of-flight PET - IOPscience Phys. Med. Biol 61 L38–47 [PubMed: 27589153]

Lecoq P, Auffray E, Brunner S, Hillemanns H, Jarron P, Knapitsch A, Meyer T and Powolny F 2010 Factors Influencing Time Resolution of Scintillators and Ways to Improve Them IEEE Trans. Nucl. Sci 57 2411–6

Lecoq P, Gektin A and Korzhik M 2016 Inorganic Scintillators for Detector Systems: Physical Principles and Crystal Engineering (Springer)

Li C, Di K, Bec J and Cherry SR 2013 X-ray luminescence optical tomography imaging: experimental studies Opt. Lett 38 2339–41 [PubMed: 23811921]

Li C, Mitchell GS and Cherry SR 2010 Cerenkov luminescence tomography for small-animal imaging Opt. Lett 35 1109 [PubMed: 20364233]

Liu H, Carpenter CM, Jiang H, Pratx G, Sun C, Buchin MP, Gambhir SS, Xing L and Cheng Z 2012 Intraoperative Imaging of Tumors Using Cerenkov Luminescence Endoscopy: A Feasibility Experimental Study J. Nucl. Med 53 1579–84 [PubMed: 22904353]

Liu H, Ren G, Miao Z, Zhang X, Tang X, Han P, Gambhir SS and Cheng Z 2010a Molecular Optical Imaging with Radioactive Probes PLOS ONE 5 e9470 [PubMed: 20208993]

Liu H, Zhang X, Xing B, Han P, Gambhir SS and Cheng Z 2010b Radiation-Luminescence-Excited Quantum Dots for in vivo Multiplexed Optical Imaging Small 6 1087–91 [PubMed: 20473988]

Madras BK, Cohen EL, Messing R, Munro HN and Wurtman RJ 1974 Relevance of free tryptophan in serum to tissue tryptophan concentrations Metabolism 23 1107–16 [PubMed: 4427559]

Maldiney T, Kaikkonen MU, Seguin J, le Masne de Chermont Q, Bessodes M, Airenne KJ, Ylä-Herttuala S, Scherman D and Richard C 2012 In Vitro Targeting of Avidin-Expressing Glioma Cells with Biotinylated Persistent Luminescence Nanoparticles Bioconjug. Chem 23 472–8 [PubMed: 22250884]

Maldiney T, Viana B, Bessière A, Gourier D, Bessodes M, Scherman D and Richard C 2013 In vivo imaging with persistent luminescence silicate-based nanoparticles Opt. Mater 35 1852–8

Matsubara T, Kusuzaki K, Matsumine A, Murata H, Nakamura T, Uchida A and Sudo A 2010 Clinical outcomes of minimally invasive surgery using acridine orange for musculoskeletal sarcomas around the forearm, compared with conventional limb salvage surgery after wide resection J. Surg. Oncol 102 271–5 [PubMed: 20740586]

Mitchell GS, Gill RK, Boucher DL, Li C and Cherry SR 2011 In vivo Cerenkov luminescence imaging: a new tool for molecular imaging Philos. Transact. A Math. Phys. Eng. Sci 369 4605–19

Monteiro CMB, Lopes JAM, Veloso JFCA and dos Santos JMF 2008 Secondary scintillation yield in pure argon Phys. Lett. B 668 167–70

Moore L. Thomas, Fenglin Wang, Hongyu Chen, Grimes W. Stuart, Anker Jeffrey N. and Frank Alexis 2014 Polymer-Coated Radioluminescent Nanoparticles for Quantitative Imaging of Drug Delivery Adv. Funct. Mater 24 5815–23

Morgan NY, Kramer-Marek G, Smith PD, Camphausen K and Capala J 2009 Nanoscintillator Conjugates as Photodynamic Therapy-Based Radiosensitizers: Calculation of Required Physical Parameters Radiat. Res 171 236–44 [PubMed: 19267550]

Morii H, Mizouchi K, Nomura T, Sasao N, Sumida T, Kobayashi M, Murayama Y and Takashima R 2004 Quenching effects in nitrogen gas scintillation Nucl. Instrum. Methods Phys. Res. Sect. Accel. Spectrometers Detect. Assoc. Equip 526 399–408

Moss SH and Smith KC 1980 Cerenkov Ultraviolet Radiation (137Cs γ-rays) and Direct Excitation (137Cs γ-rays and 50 kVp X-rays) Produce Photoreactivable Damage in Escherichia Coli Int. J. Radiat. Biol. Relat. Stud. Phys. Chem. Med 38 323–34 [PubMed: 7012061]

Naczynski DJ, Sun C, Türkcan S, Jenkins C, Koh AL, Ikeda D, Pratx G and Xing L 2015 X-ray-Induced Shortwave Infrared Biomedical Imaging Using Rare-Earth Nanoprobes Nano Lett 15 96–102 [PubMed: 25485705]

Nelson DR, Carter JG, Birkhoff RD, Hamm RN and Augenstein LG 1967 Yield of Luminescence from X-Irradiated Biochemicals Radiat. Res 32 723–43 [PubMed: 6066588]

Niedre MJ, Secord AJ, Patterson MS and Wilson BC 2003 In Vitro Tests of the Validity of Singlet Oxygen Luminescence Measurements as a Dose Metric in Photodynamic Therapy Cancer Res 63 7986–94 [PubMed: 14633731]

Nikolopoulos D, Valais I, Michail C, Bakas A, Fountzoula C, Cantzos D, Bhattacharyya D, Sianoudis I, Fountos G, Yannakopoulos P, Panayiotakis G and Kandarakis I 2016 Radioluminescence properties of the CdSe/ZnS Quantum Dot nanocrystals with analysis of long-memory trends Radiat. Meas 92 19–31

Ochsner M 1997 Photophysical and photobiological processes in the photodynamic therapy of tumours J. Photochem. Photobiol. B 39 1–18 [PubMed: 9210318]

Osakada Y, Pratx G, Hanson L, Solomon PE, Xing L and Cui B 2013 X-ray excitable luminescent polymer dots doped with an iridium(iii) complex Chem. Commun 49 4319–21

Osakada Y, Pratx G, Sun C, Sakamoto M, Ahmad M, Volotskova O, Ong Q, Teranishi T, Harada Y, Xing L and Cui B 2014 Hard X-ray-induced optical luminescence via biomolecule-directed metal clusters Chem. Commun 50 3549–51

Ouyang Z, Liu B, Yasmin-Karim S, Sajo E and Ngwa W 2016 Nanoparticle-aided external beam radiotherapy leveraging the Čerenkov effect Phys. Med 32 944–7 [PubMed: 27397906]

Palner M, Pu K, Shao S and Rao J 2015 Semiconducting Polymer Nanoparticles with Persistent Near-Infrared Luminescence for In Vivo Optical Imaging Angew. Chem 127 11639–42

Patterson MS, Wilson BC and Graff R 1990 In vivo tests of the concept of photodynamic threshold dose in normal rat liver photosensitized by aluminum chlorosulphonated phthalocyanine Photochem. Photobiol 51 343–9 [PubMed: 2356229]

Pogue BW, Feng J, LaRochelle EP, Bruža P, Lin H, Zhang R, Shell JR, Dehghani H, Davis SC, Vinogradov SA, Gladstone DJ and Jarvis LA 2018 Maps of in vivo oxygen pressure with submillimetre resolution and nanomolar sensitivity enabled by Cherenkov-excited luminescence scanned imaging Nat. Biomed. Eng 2 254–64 [PubMed: 30899599]

Pogue BW and Wilson BC 2018 Optical and x-ray technology synergies enabling diagnostic and therapeutic applications in medicine J. Biomed. Opt 23 121610

Pratt EC, Shaffer TM, Zhang Q, Drain CM and Grimm J 2018 Nanoparticles as multimodal photon transducers of ionizing radiation Nat. Nanotechnol 1

Pratx G 2017 A tale of two photons: radioluminescence and its application in molecular imaging Molecular-Guided Surgery: Molecules, Devices, and Applications III Molecular-Guided Surgery: Molecules, Devices, and Applications III vol 10049 (International Society for Optics and Photonics) p 1004916 Online: https://www.spiedigitallibrary.org/conference-proceedings-of-spie/10049/1004916/A-tale-of-two-photons--radioluminescence-and-its-application/10.1117/12.2256702.short

Pratx G, Carpenter CM, Sun C, Rao RP and Xing L 2010a Tomographic molecular imaging of x-ray-excitable nanoparticles Opt. Lett 35 3345–7 [PubMed: 20967061]

Pratx G, Carpenter CM, Sun C and Xing L 2010b X-Ray Luminescence Computed Tomography via Selective Excitation: A Feasibility Study IEEE Trans. Med. Imaging 29 1992–9 [PubMed: 20615807]

Pratx G, Chen K, Sun C, Axente M, Sasportas L, Carpenter C and Xing L 2013 High-Resolution Radioluminescence Microscopy of 18F-FDG Uptake by Reconstructing the β-Ionization Track J. Nucl. Med 54 1841–6 [PubMed: 24003077]

Pratx G, Chen K, Sun C, Martin L, Carpenter CM, Olcott PD and Xing L 2012 Radioluminescence Microscopy: Measuring the Heterogeneous Uptake of Radiotracers in Single Living Cells PLOS ONE 7 e46285 [PubMed: 23056276]

Quickenden TI 1971 The Luminescence of Water Excited by Ambient Ionizing Radiation Radiat. Res 46 28–35 [PubMed: 5574241]

Rao P, VL; Radiobioluminescence, cerenkov luminescence-God light in likes, a potential in radiation therapy imaging. 2015. Online: http://www.cancerjournal.net/article.asp?issn=0973-1482;year=2015;volume=11;issue=1;spage=241;epage=242;aulast=Rao

Robertson R, Germanos MS, Li C, Mitchell GS, Cherry SR and Silva MD 2009 Optical imaging of Cerenkov light generation from positron-emitting radiotracers Phys. Med. Biol 54 N355–65 [PubMed: 19636082]

Rowlands JA. 2002; The physics of computed radiography. Phys. Med. Biol. 47:R123. [PubMed: 12502037]

Ruggiero A, Holland JP, Lewis JS and Grimm J 2010 Cerenkov Luminescence Imaging of Medical Isotopes J. Nucl. Med 51 1123–30 [PubMed: 20554722]

Sanderson DCW, Slater C and Cairns KJ 1989 Thermoluminescence of foods: Origins and implications for detecting irradiation Int. J. Radiat. Appl. Instrum. Part C Radiat. Phys. Chem 34 915–24

Scaffidi JP, Gregas MK, Lauly B, Zhang Y and Vo-Dinh T 2011 Activity of Psoralen-Functionalized Nanoscintillators against Cancer Cells upon X-ray Excitation ACS Nano 5 4679–87 [PubMed: 21553850]

Schwarz HA. 1981; Free radicals generated by radiolysis of aqueous solutions. J. Chem. Educ. 58:101.

Sengupta D and Pratx G 2016 Single-cell characterization of FLT uptake with radioluminescence microscopy J. Nucl. Med. jnumed 115167734

Shaffer TM, Pratt EC and Grimm J 2017 Utilizing the power of Cerenkov light with nanotechnology Nat. Nanotechnol 12 106–17 [PubMed: 28167827]

Sharpatyi VA and Kraljić I 1978 Detection of Singlet Oxygen in Radiolysis of Aerated Aqueous Solutions Photochem. Photobiol 28 587–90

Sicard-Roselli C, Brun E, Gilles M, Baldacchino G, Kelsey C, McQuaid H, Polin C, Wardlow N and Currell F 2014 A New Mechanism for Hydroxyl Radical Production in Irradiated Nanoparticle Solutions Small 10 3338–46 [PubMed: 24863679]

Sitharamarao DN and Duncan JF 1963 Molecular Excitation of Water by $gamma$-Irradiation J. Phys. Chem. US Vol: 67 Online: https://www.osti.gov/scitech/biblio/4633308

Soika C and Delincée H 2000 Thermoluminescence Analysis for Detection of Irradiated Food—Luminescence Characteristics of Minerals for Different Types of Radiation and Radiation Doses LWT - Food Sci. Technol 33 431–9

Liang Song, Pei-Pei Li, Wen Yang, Xia-Hui Lin, Hong Liang, Xiao-Feng Chen, Gang Liu, Juan Li and Huang-Hao Yang 2018 Low-Dose X-ray Activation of W(VI)-Doped Persistent Luminescence Nanoparticles for Deep-Tissue Photodynamic Therapy Adv. Funct. Mater 0 1707496

Spinelli AE, Calandrino R, Meo SL, Sbarbati A and Boschi F 2011 Optical imaging of Tc-99m-based tracers: in vitro and in vivo results J. Biomed. Opt 16 116023 [PubMed: 22112128]

Spinelli AE, Ferdeghini M, Cavedon C, Zivelonghi E, Calandrino R, Fenzi A, Sbarbati A and Boschi F 2013 First human Cerenkography J. Biomed. Opt 18 020502–020502

Suzuki M and Kubota S 1979 Mechanism of proportional scintillation in argon, krypton and xenon Nucl. Instrum. Methods 164 197–9

Tanha K, Pashazadeh AM and Pogue BW 2015 Review of biomedical Čerenkov luminescence imaging applications Biomed. Opt. Express 6 3053–65 [PubMed: 26309766]

Tarasov MD, El'yash SL, Goncharova VF, Petrushin ON, Savel'ev YA, Tarakanov MY and Shigaev YS 2007 Efficiency of radioluminescence of water under the action of accelerated electrons Instrum. Exp. Tech 50 761–3

Butterworth K T, McMahon S J, Currell F J and Prise K M 2012 Physical basis and biological mechanisms of gold nanoparticle radiosensitization Nanoscale 4 4830–8 [PubMed: 22767423]

Thorek DLJ, Das S and Grimm J 2014a Molecular Imaging Using Nanoparticle Quenchers of Cerenkov Luminescence Small 10 3729–34 [PubMed: 24861843]

Thorek DLJ, Ogirala A, Beattie BJ and Grimm J 2013 Quantitative imaging of disease signatures through radioactive decay signal conversion Nat. Med 19 1345–50 [PubMed: 24013701]

Thorek DLJ, Riedl CC and Grimm J 2014b Clinical Cerenkov Luminescence Imaging of 18F-FDG J. Nucl. Med 55 95–8 [PubMed: 24078721]

US EPA O. Climate Change Indicators: Atmospheric Concentrations of Greenhouse Gases US EPA. 2016. Online: https://www.epa.gov/climate-indicators/climate-change-indicators-atmospheric-concentrations-greenhouse-gases

Van den Eeckhout K, Smet PF and Poelman D 2010 Persistent Luminescence in Eu2+-Doped Compounds: A Review Materials 3 2536–66

Vasil'ev RF. 1970; Chemiluminescence Excitation Mechanisms. Russ. Chem. Rev. 39:529.

Volotskova O, Sun C, Stafford JH, Koh AL, Ma X, Cheng Z, Cui B, Pratx G and Xing L 2015 Efficient Radioisotope Energy Transfer by Gold Nanoclusters for Molecular Imaging Small 11 4002–8 [PubMed: 25973916]

Wang C, Volotskova O, Lu K, Ahmad M, Sun C, Xing L and Lin W 2014 Synergistic Assembly of Heavy Metal Clusters and Luminescent Organic Bridging Ligands in Metal–Organic Frameworks for Highly Efficient X-ray Scintillation J. Am. Chem. Soc 136 6171–4 [PubMed: 24730683]

Wang Q, Sengupta D, Kim TJ and Pratx G 2017 Performance evaluation of 18F radioluminescence microscopy using computational simulation Med. Phys 44 1782–95 [PubMed: 28273348]

Weston MA and Patterson MS 2008 Simple Photodynamic Therapy Dose Models Fail to Predict the Survival of MLL Cells After HPPH–PDT In Vitro Photochem. Photobiol 85 750–9 [PubMed: 19140895]

Wilson BC and Patterson MS 1986 The physics of photodynamic therapy Phys. Med. Biol 31 327 [PubMed: 3526361]

Yaffe MJ and Rowlands JA 1997 X-ray detectors for digital radiography Phys. Med. Biol 42 1 [PubMed: 9015806]

Yamamoto S, Koyama S, Komori M and Toshito T 2016 Luminescence imaging of water during irradiation of X-ray photons lower energy than Cerenkov- light threshold Nucl. Instrum. Methods Phys. Res. Sect. Accel. Spectrometers Detect. Assoc. Equip 832 264–70

Yoon SW, Tsvankin V, Shrock Z, Meng B, Zhang X, Dewhirst M, Fecci P, Adamson J and Oldham M 2017 Enhancing Radiation Therapy through Cherenkov Light Activated Phototherapy Int. J. Radiat. Oncol Online: http://www.sciencedirect.com/science/article/pii/S0360301617341226

Zhang R, D'souza AV, Gunn JR, Esipova TV, Vinogradov SA, Glaser AK, Jarvis LA, Gladstone DJ and Pogue BW 2015 Cherenkov-excited luminescence scanned imaging Opt. Lett 40 827–30 [PubMed: 25723443]

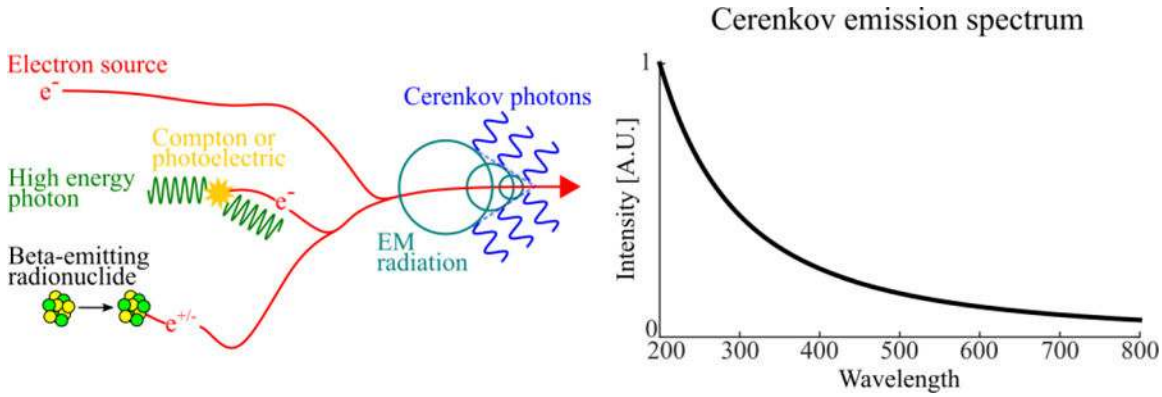

Figure 1.

Physics of Cerenkov photon production (left) and emission spectrum (right). Cerenkov photons can be produced by a variety of medical sources including: linear accelerators (linacs) emitting megavoltage electrons or photons, and beta-emitting radionuclides used in radiopharmaceuticals. The emission spectrum is continuous from the ultraviolet to infrared with intensity proportional to λ^{-2}

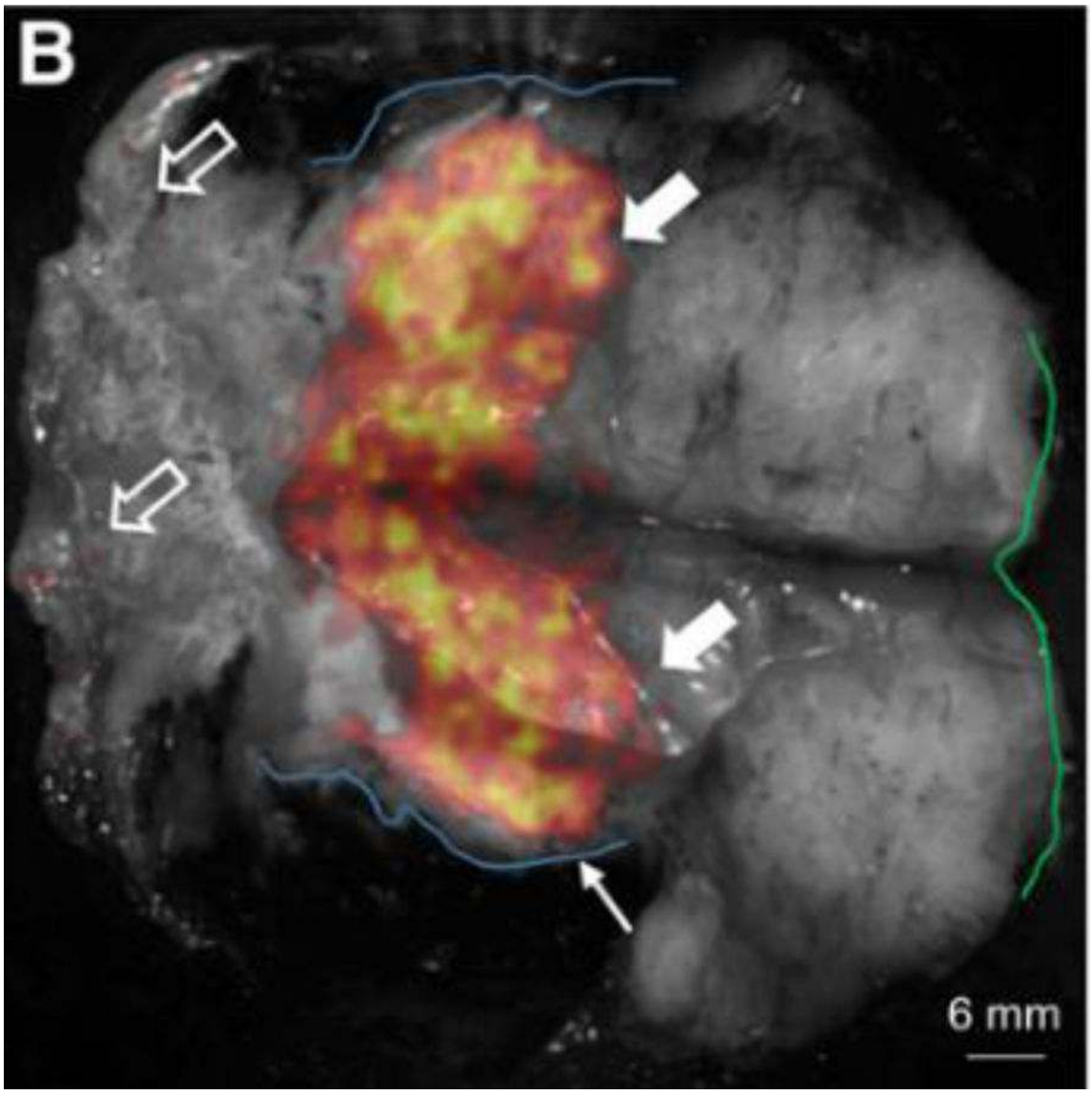

Figure 2.

Ex vivo specimen imaging of excised breast tissue. Black and white is reflectance tissue image and overlaid heatmap is CL image. This research was originally published in JNM. Grootendorst M. R. et al. A 2016 Intraoperative Assessment of Tumor Resection Margins in Breast-Conserving Surgery using ^{18}F-FDG Cerenkov Luminescence Imaging – A First-in-Human Feasibility Study. J Nucl Med. 2016. Jun;58(6):891–898. © SNMMI.

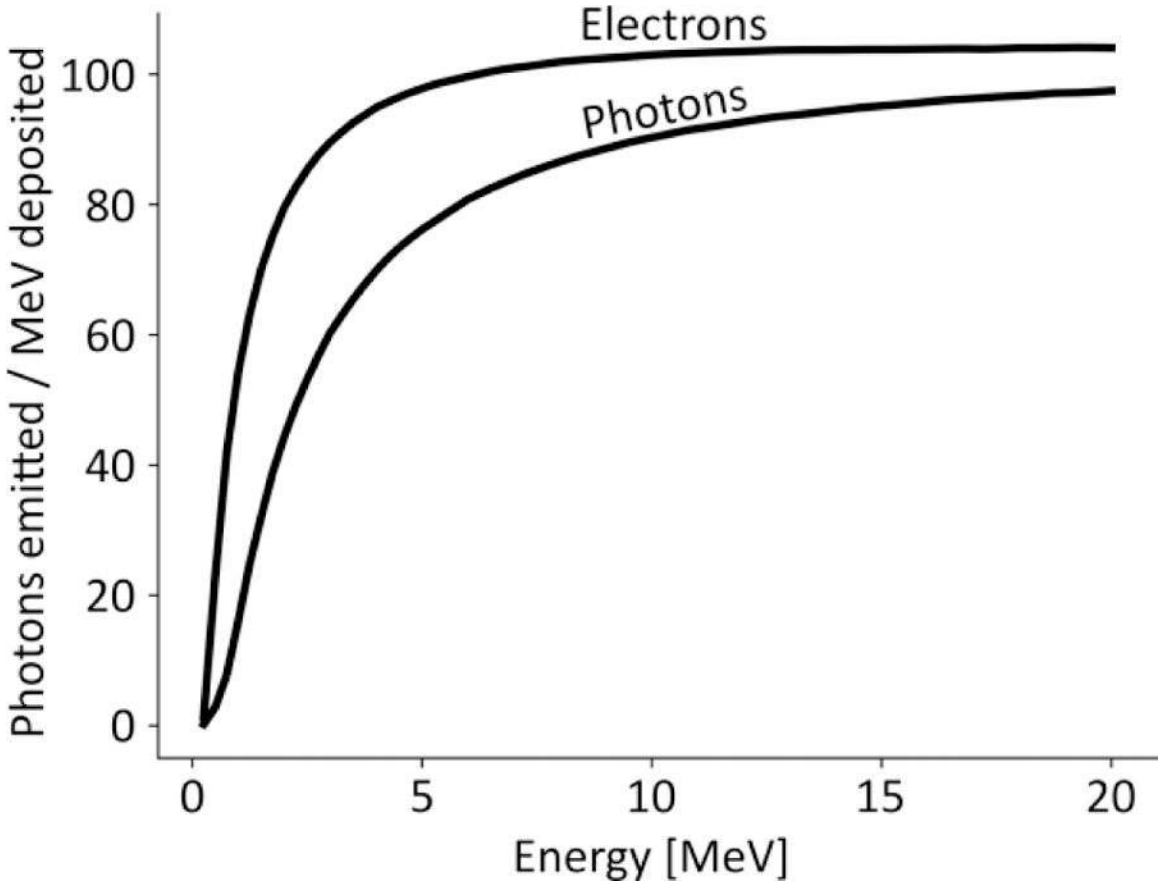

Figure 3.

Estimated Cerenkov photon yield (R_E) per energy deposited from photons and electron beams. Data are adapted from Glaser et al 2014

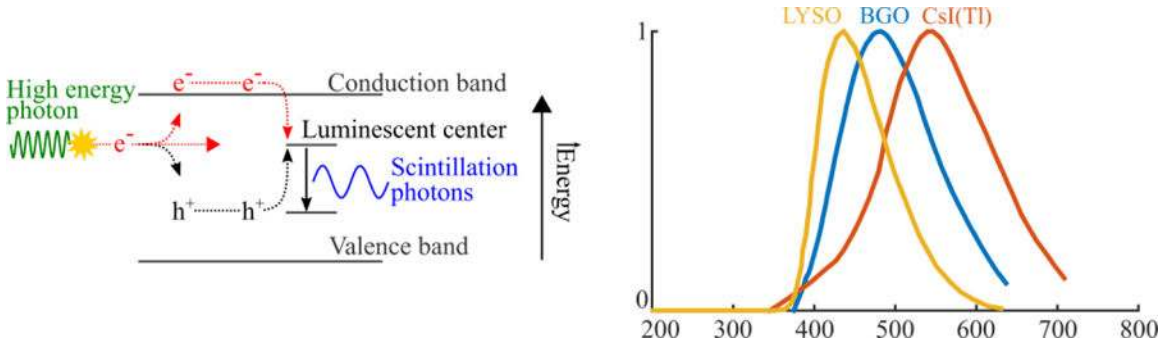

Figure 4.

Physics of inorganic scintillation (left) and typical emission spectra for common scintillators (right). Ionizing radiation deposits energy in the scintillator, generating mobile electron-hole pairs that produce scintillation photons when they recombine in luminescent center.

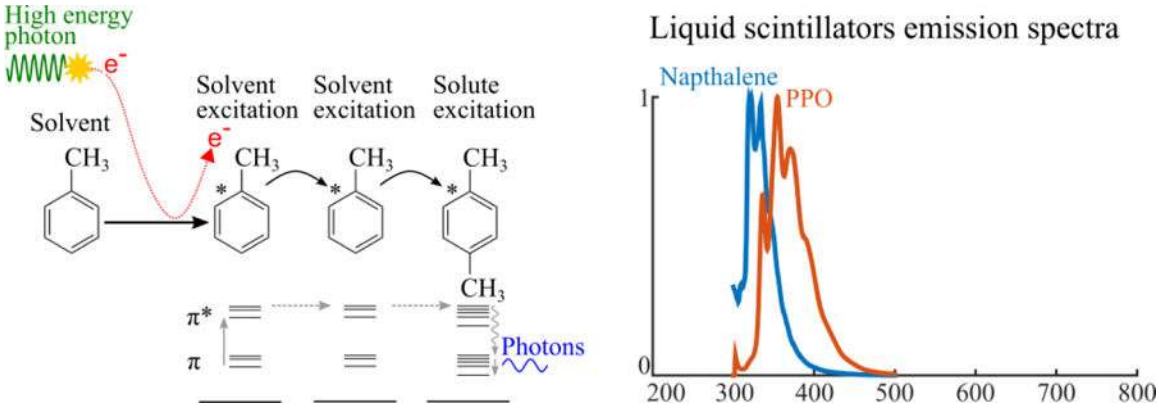

Figure 5.

Physics of organic scintillators (left) and emission spectra (right). Primary or secondary charged particles deposit energy in the solvent, exciting solvent molecules. Excitation energy transfers non-radiatively from solvent to solvent molecule. Luminescence is produced when excitation energy is transferred to a solute molecule.

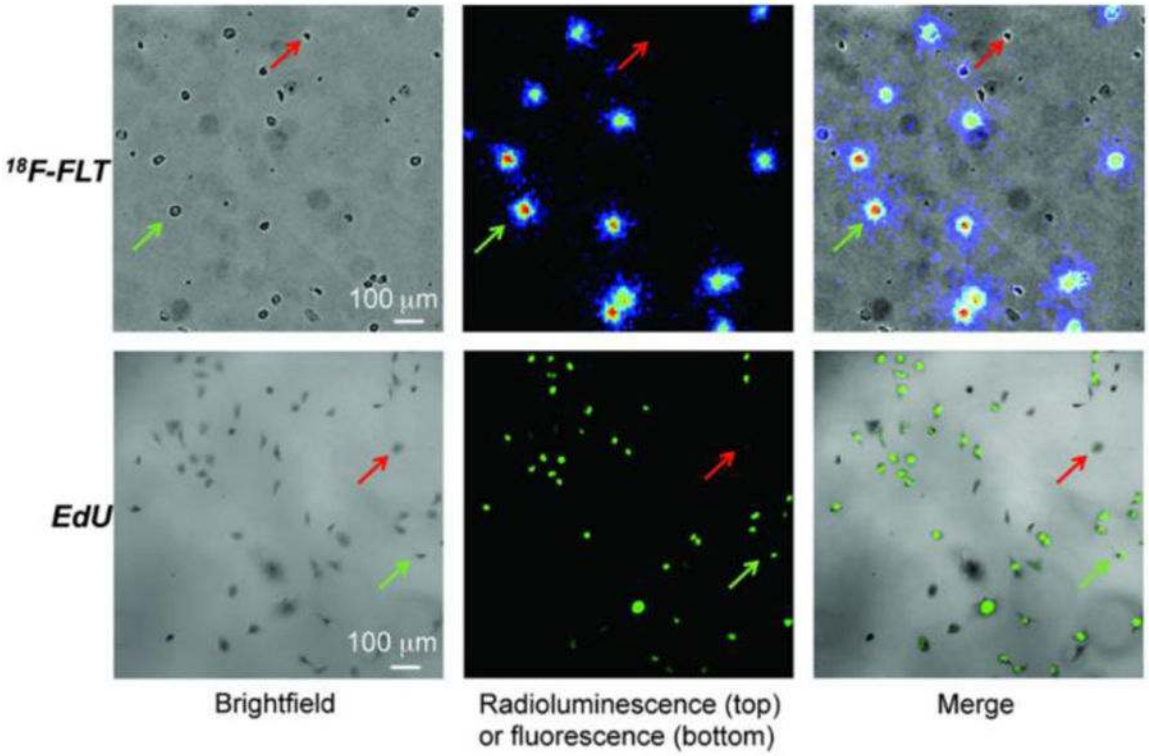

Figure 6.

MDA-MB-231 cells imaged using ^{18}F-FLT RLM and EdU fluorescence microscopy. This research was originally published in JNM. Sengupta, D. and Pratx, G. Single-cell characterization of FLT uptake with radioluminescence microscopy. J Nucl Med. 2016;Jul; 57(7):1136–40. © SNMMI

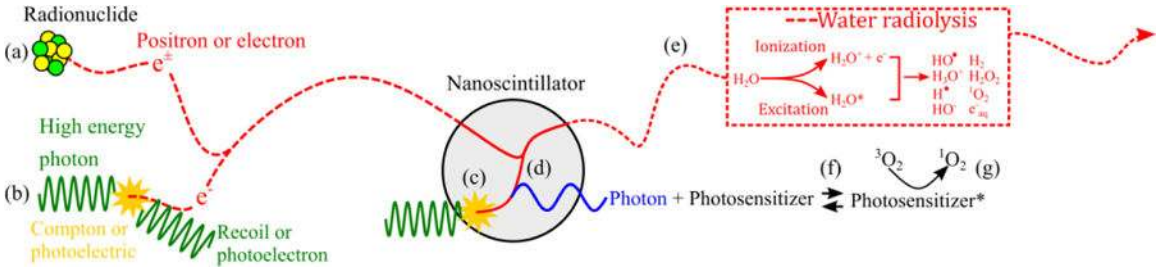

Figure 7.

Physics of ionizing radiation interacting in scintillator-containing tissue. Electrons or positrons are emitted into tissue via (a) beta-emitting radionuclides or (b) as recoil or photoelectrons from the interactions of high-energy photons with tissue. Electrons or positrons passing through tissue generate reactive species through water radiolysis (e). Photons can directly interact in the nanoscintillator, generating electrons through Compton or photoelectric absorption (c). Electrons generated in tissue (a,b) or nanoscintillator (c) deposit a small fraction of their energy in nanoscintillators, producing scintillation photons (d). Scintillation photons absorbed by the photosensitizer (f) can generate singlet oxygen or other reactive oxygen species (g). The range of ionizing particles is several orders of magnitude larger than the diameter of nanoscintillators.

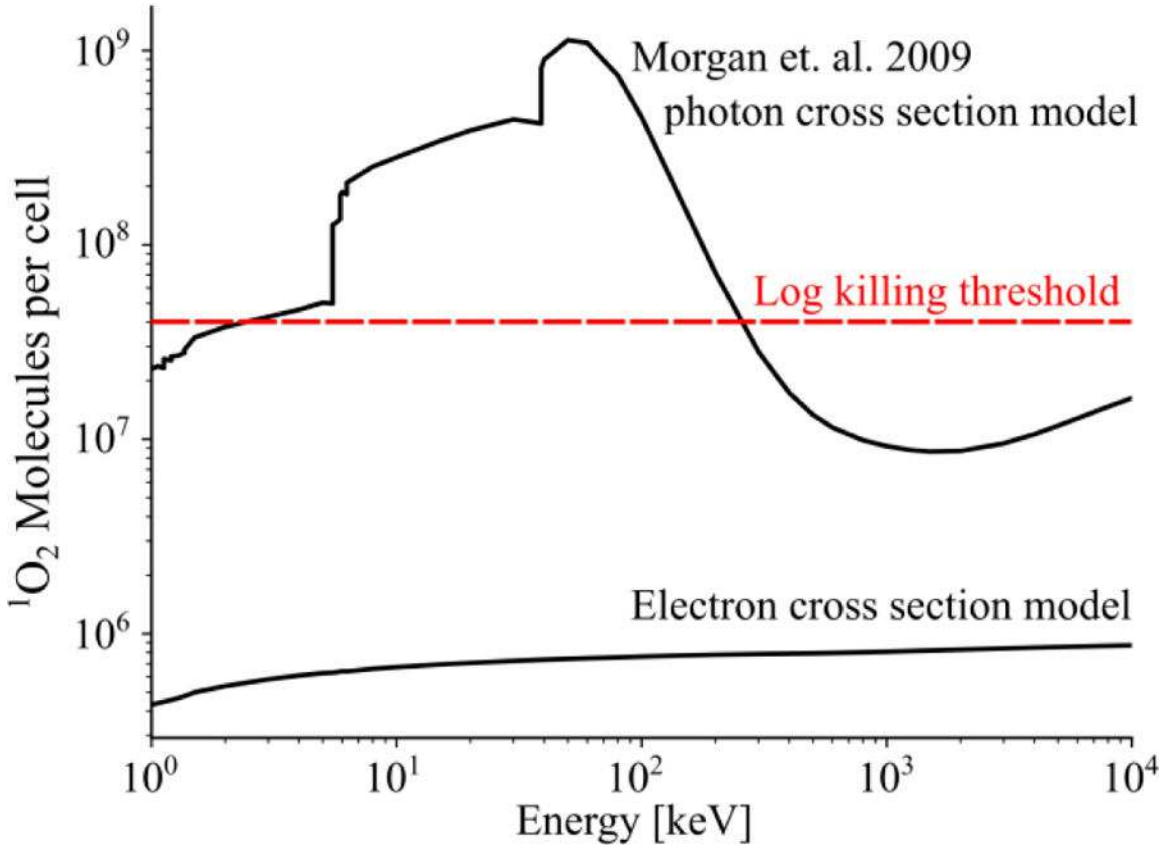

Figure 8.

Estimated molecules of O_2 generated per cell for a 60 Gy photon dose. Models that use either photon or electron cross secitons are plotted, along with an established log killing threshold (dashed).

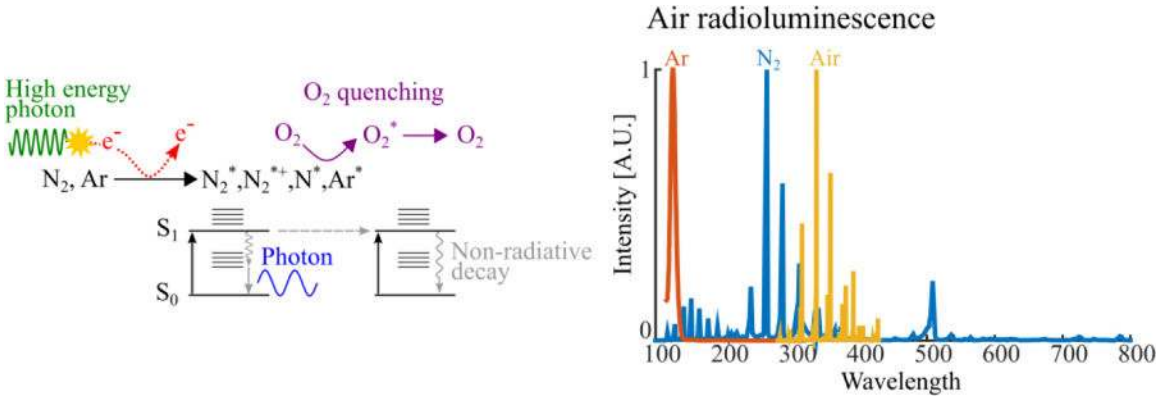

Figure 9.

Air fluorescence physics (left) and emission spectra (right). Electrons generated from the interaction of ionizing radiation with air generates electrons that excite its fluorescent constituents (primarily N_2).

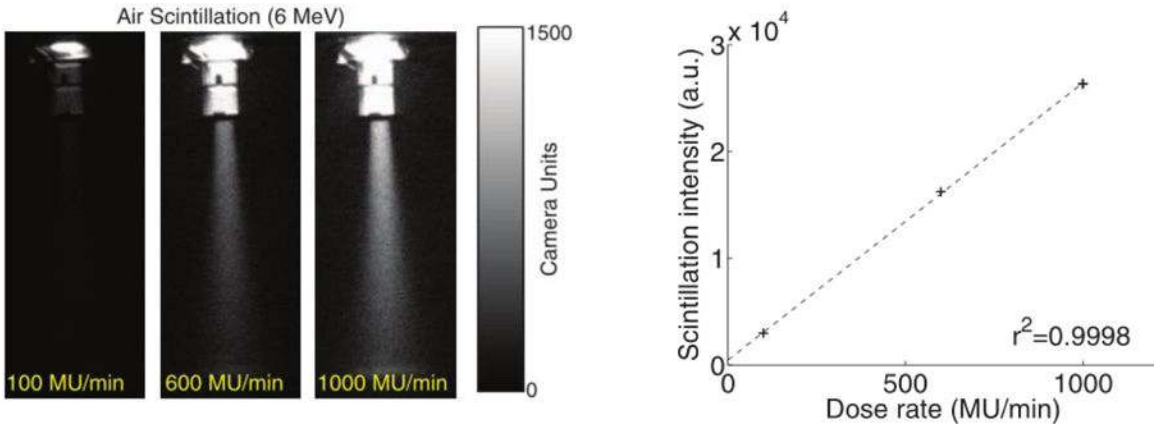

Figure 10.

Air fluorescence images from a 6 MeV electron beam at various dose rates (left) and linear relationship between fluorescence intensity and dose rate (right), from Fahimian et al 2014.

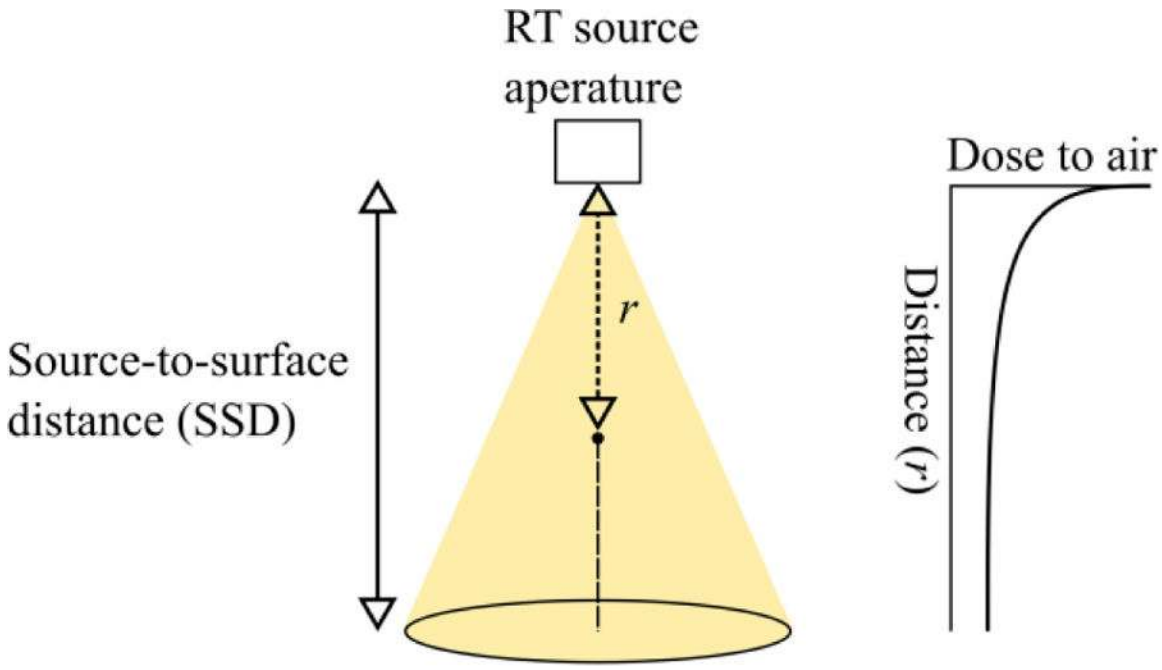

Figure 11.
Air fluorescence radiotherapy geometry. Dose to air falls with the inverse square of the distance from source (right).

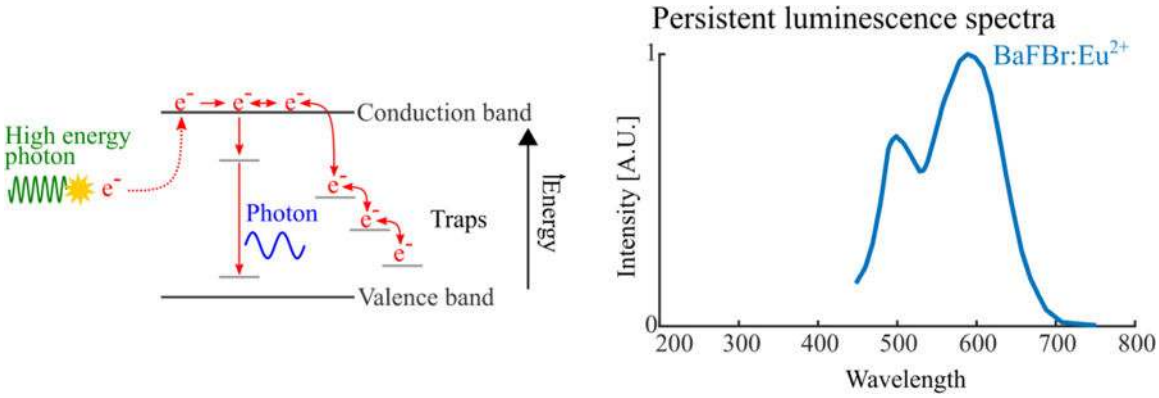

Figure 12.

Persistent luminescence physics (left) and spectra of fluorescence and persistently luminescent biological molecules (right). Absorption of energy excites electrons into the conduction band of the persistent luminescent material. Electrons can fall into traps and also return to the conduction band, eventually leading to luminescence.

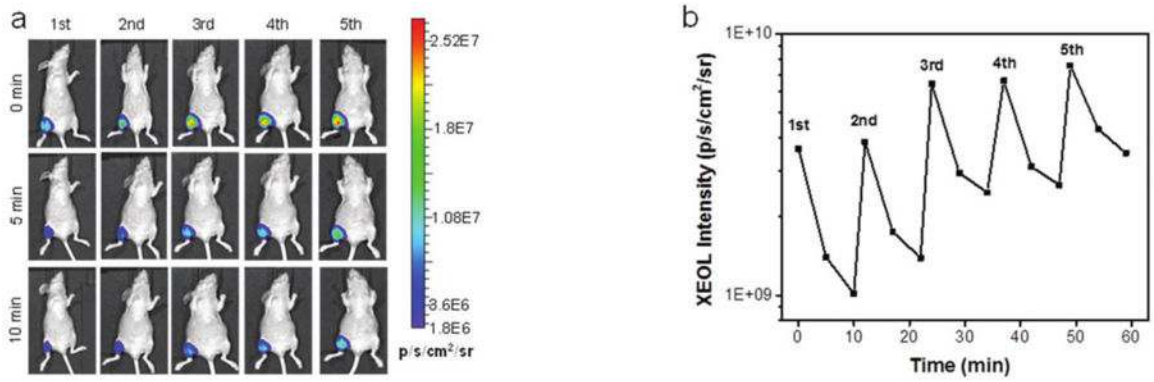

Figure 13.

Imaging (left) of repeated x-ray activation of persistent luminescence nanoparticles in vivo and ROI quantitation following repeated excitation (right) from Chen et al 2017.

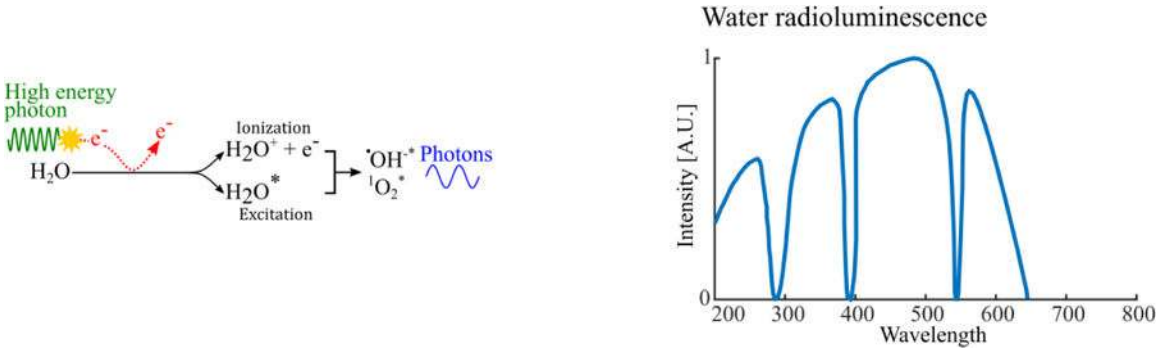

Figure 14.

Water radioluminesce physics (left) and typical spectrum (right). In pure water, radioluminescence is induced by excitation of water and water-radiolysis products by ionizing radiation.

Table 1:

Estimated photon yield and expected dose in tissue from various radionuclides.

Radionuclide	Half-life [s]	Average emitted beta energy (E_{mean}) [MeV/decay]	Cerenkov yield, 400 – 800 nm [photons/decay]	Decay factor [decays/Bq]	Decay-adjusted Cerenkov yield [photons/Bq]
^{18}F	6,582	0.242	1.32	9,478	12,511
^{64}Cu	45,723	0.060	0.56	36,278	25,605
^{68}Ga	4,070	0.735	33.9	5,861	198,688
^{89}Zr	282,240	0.198	2.29	406,426	646,330
^{90}Y	230,400	0.934	47.3	331,776	10,897,920

Table 2:

Summary of reports of radionuclide-induced Cerenkov-activated photodynamic therapy.

Reference	Source	Photosensitizer	Condition	Outcome	Cerenkov photon yield per cell (200 – 800 nm)	Estimated Cerenkov PDT effect [% tumor cells killed]	Estimated dose from radionuclide [Gy]
Kotagiri *et al* 2015	^{18}F	TiO-Tf-Tc	I.V. injection 2x; HT1080 mouse tumor	Median survival increased from 15 to 50 days	1.0×10^5	0.25	235
	^{18}F	TiO-Tf-Tc	I.V. injection 2x; A549 mouse tumor	~6.5-fold tumor growth inhibition at day 30 compared to control	1.0×10^5	0.25	235
	^{64}Cu	TiO-Tf-Tc	Direct tumor injection; HT1080 mouse tumor	Complete regression at 30 days	4.2×10^4	0.11	117
Kamkaew *et al* 2016 ‡	^{89}Zr	HMSN-Ce6	Direct injection; 4T1 mouse tumor	Tumor growth completely inhibited within 14 days post-injection	8.6×10^5	2.13	973
Hartl *et al* 2016 †	^{90}Y	$TPPS_{2a}$	In vitro; C6 cells	Cell viability decreased ~22% compared to radiation effect alone	1.4×10^7	29.6	592
Nakamura *et al* 2017	^{18}F	pan-IR700 (panitumumab conjugated to IR700 dye)	In vitro; A431-luc cells	Decreased A431-luc bioluminescence in dose-dependent manner (*in vitro*); no significant long-term therapeutic effect (*in vivo*)	4.13×10^2	0	4

‡Expected photon yield, PDT effect, and radiation dose computed using 14 day experiment duration

†Expected photon yield, PDT effect, and radiation dose computed using 72 hour reported incubation period

Table 3:

Summary of reports of Cerenkov-activated radiotherapy induced photodynamic therapy

Reference	X-ray energy [MV]	Photosensitizer	Condition	Outcome	Cerenkov photons absorbed per cell (200– 800 nm)	Estimated Cerenkov PDT effect [% tumor cells killed]	Reported dose to cell layer [Gy]
Ouyang *et al* 2016	6	TiO_2 anatase nanoparticles	In vitro, A549	Decreased colony formation by ~20% compared to radiation group alone	3.7×10^6	8.88	2
Yoon *et al* 2017 *	6	Psoralen	In vitro, B16 & 4T1	Decreased colony formation of 20% and 9.5% for 4T1 and B16 cells, respectively	2.8×10^5	0.69	12

* Solid-water slab not included in model

Table 4:

Estimated photon yield from 1 mg/cm^3 LaF_3 nanoscintillator in tissue receiving 1 Gy radiation dose using different photon energies

Photon energy [MV]	Electron mass attenuation coefficient [MeV·cm^2/g]		Photons emitted	
	LaF_3	Tissue	Photons / cm^3	Photons / MeV deposited
0.001	41.9	121	2.15×10^{11}	34
0.01	12.3	22.6	3.37×10^{11}	54
0.1	2.55	4.11	3.85×10^{11}	62
1	1.26	1.85	4.22×10^{11}	68
10	2.09	2.13	6.08×10^{11}	97

Table 5:

Energy deposited in air and computed luminescence from 6 and 10 MeV electrons or photons emitted from a radiotherapy source.

Energy [MeV]	Particle type	Mass-energy attenuation coefficient [cm^2/g or $MeV \cdot cm^2/g$]		Dose to air (r = 50 cm) per 1 Gy dose to tissue (SSD = 100 cm) [Gy]	Photons generated (SSD = 50 cm) [$photons/cm^3$]
		Air	Tissue		
6	Photon	0.0165	0.0179	3.69	7.00×10^8
10	Photon	0.0145	0.0155	3.74	7.11×10^8
6	e^-	1.97	2.00	3.94	7.49×10^8
10	e^-	2.16	2.13	4.05	7.69×10^8

Table 6:

Summary of radioluminescent sources

Source	Photon yield (photons / MeV energy deposited)			Spectral range (nm)	Mechanism	References
Inorganic scintillators	10^4 – 10^5			400 – 600	Scintillation	(Cherry *et al* 2012)
Organic scintillators	10^4			300 – 450	Fluorescence / phosphorescence	(Birks 1964)
Liquid scintillators	10^4			300 – 450	Fluorescence / phosphorescence	(Horrocks 1974)
Air scintillation	N_2	120		100 – 500 (peaks)	Ionization / fluorescence	(Suzuki and Kubota 1979, Morii *et al* 2004)
	O_2	<1 (quencher)				
	Ar	10^4				
	Air	25				
Cerenkov radiation	Radionuclides	1 – 100 (decay^{-1})		200 – 800	Cerenkov radiation	(Ackerman and Graves 2012, Gill *et al* 2015)
	Radiotherapy	6 MeV e^-	100	200 – 800	Cerenkov radiation	(Glaser *et al* 2014)
		10 MeV e^-	103			
		6 MeV photon	81			
		10 MeV photon	91			
Nanoparticle scintillators (1 mg/cm^3)	10 – 100			400 – 600	Scintillation	(Bulin *et al* 2015)
Endogenous biological molecules (Tyrosine, Trypsin, Phenylalanine, Tryptophan) †	Immediate	Thermo-luminescence		300 – 600	Fluorescence / persistent luminescence	(Nelson *et al* 1967)
	8×10^3 - 6×10^4	4.5 – 310				
Water radioluminescence	< 1			200 – 600 (500 peak)	Fluorescence	(Tarasov *et al* 2007)

†Reported values are for molecules in their pure, crystalized form; typical concentrate is ~μg/cm^3 *in vivo* (Madras *et al* 1974)